Development of Braided Peltier Devices to Achieve Thermoelectric Cooling in Shape Memory Alloy Actuation Mechanisms

Cynthia Xinjia Wang
Student number: 02302048

Supervisor: Dr. ir. Johannes Mersch
Counsellor: Dr. ir. Marie Janssens
Examiner: Prof. dr. Chokri Cherif and Associate Prof. dr. Narantogtokh Davaajav

Master's thesis submitted under the framework of WE-TEAM: World Textile Engineering Advanced Master, affiliated with the Institute of Textile Machinery and High Performance Material Technology (ITM) at the Dresden University of Technology, Germany, in order to obtain the academic degree of

International Master of Science in Textile Engineering from Ghent University, Belgium
Master of Engineering from Kyoto Institute of Technology, Japan
Master in Mechanic and Fibrous Materials from University of Haute-Alsace, France
Master of Science in Textile Engineering from Universitat Politècnica de Valencia, Spain

Academic year: 2024-2025
Date: 2025/06/11

This page is intentionally left blank.

This page is intentionally left blank.

Development of Braided Peltier Devices to Achieve Thermoelectric Cooling in Shape Memory Alloy Actuation Mechanisms

Cynthia Xinjia Wang
Student number: 02302048

Supervisor: Dr. ir. Johannes Mersch
Counsellor: Dr. ir. Marie Janssens
Examiner: Prof. dr. Chokri Cherif and Associate Prof. dr. Narantogtokh Davaajav

Master's thesis submitted under the framework of WE-TEAM: World Textile Engineering Advanced Master, affiliated with the Institute of Textile Machinery and High Performance Material Technology (ITM) at the Dresden University of Technology, Germany, in order to obtain the academic degree of

International Master of Science in Textile Engineering from Ghent University, Belgium
Master of Engineering from Kyoto Institute of Technology, Japan
Master in Mechanic and Fibrous Materials from University of Haute-Alsace, France
Master of Science in Textile Engineering from Universitat Politècnica de Valencia, Spain

Academic year: 2024-2025
Date: 2025/06/11

Acknowledgements

I would like to use this space to express some of the people who have helped me on this thesis project. Each of the people here elevated my experience during these past five months, and had a part in shaping what this project has become. For that, I am grateful.

I would like to express my sincere gratitude to my thesis supervisor, Dr. Johannes Mersch, for his invaluable guidance, support, and encouragement throughout this project. I am equally grateful to Dr. Enrico Sommer for supervising my fibre experiments in the Dresden-Dobritz chemical lab twice a month; his insights and feedback have been instrumental in shaping the direction of this work. I would also like to thank Professor Chokri Cherif and Associate Professor Narantogtokh Davaajav for serving as members of the assessment committee for this thesis.

I am deeply thankful to my colleagues in the SMA group, especially Dr. Hung Le Xuan for his wealth of information on the CeTi project and for having lots of forward-thinking ideas that greatly influenced my approach. I would like to thank the wider ITM community, particularly Benny Waschilewski, Mathis Bruns, Nadja Schenk, Martin Kern, Florian Schmidt, Fei Sun, Jakob Mehlzer, and Carmen Sachse for helpful discussions, technical advice, and camaraderie that enriched my research experience. Special thanks are due to the technical staff at ITM: Thomas Bahr, Andre Chill, Quan Dang Hong, and Sebastian Berndt for their indispensable assistance with equipment and fabrication processes, and for tolerating my frequent scavenging missions in the ITM warehouse for parts.

I would also like to extend my heartfelt thanks to the management team and my fellow participants in the WE-TEAM programme. It has been a rewarding journey for all nineteen of us. I am especially grateful to Professor Lieva Van Langenhove and Dr. Benny Malengier, whose courses were truly formative in shaping how I approach academic work. A paper I first encountered in Professor Van Langenhove's class last year, a paper they co-authored about textile thermoelectric generators was a major inspiration for this thesis.

Lastly and most importantly, I wish to thank my family and friends for their unwavering support and encouragement throughout my studies.

Cynthia Xinjia Wang
2025/06/11

This page is intentionally left blank.

Admission to loan

Toegang tot bruikleen

Cynthia Xinjia Wang, June 2025

This page is intentionally left blank.

Development of Braided Peltier Devices to Achieve Thermoelectric Cooling in Shape Memory Alloy Actuation Mechanisms

by
Cynthia Xinjia Wang

Master's thesis submitted under the framework of WE-TEAM: World Textile Engineering Advanced Master, affiliated with the Institute of Textile Machinery and High Performance Material Technology (ITM) at the Dresden University of Technology, Germany, in order to obtain the academic degree of
International Master of Science in Textile Engineering from Ghent University, Belgium
Master of Engineering from Kyoto Institute of Technology, Japan
Master in Mechanic and Fibrous Materials from University of Haute-Alsace, France
Master of Science in Textile Engineering from Universitat Politècnica de Valencia, Spain

Supervisor: Dr. ir. Johannes Mersch
Counsellor: Dr. ir. Marie Janssens

Ghent University

Department of Materials, Textiless And Chemical Engineering

Abstract - This dissertation investigates the design and development of braided Peltier devices for achieving active thermoelectric cooling in shape memory alloy (SMA) actuation mechanisms. The research focuses on the integration of periodically nickel-electroplated thermoelectric fibres into flexible braided textile structures that thermally couple and act as a sheath to SMA wires. By leveraging the Peltier effect within the braid architecture, the system is designed to enhance the thermal management and dynamic response of the SMA-based actuators. The work includes fibre fabrication, braid prototyping, electrical and thermal characterisation, and performance testing of the integrated thermoelectric-SMA smart textile. Results indicate that while passive thermoelectric integration modestly improves actuation timing and force response, active Peltier cooling alone was unable to overcome the dominant effects of Joule heating in the current system. Nonetheless, the trends observed suggest potential for improving thermal management in smart textile systems through enhanced thermoelectric design. The findings contribute to the advancement of flexible, textile-integrated thermoelectric devices and their application in wearables and responsive materials.

Keywords - Smart Textiles, Thermoelectric Cooling, Braided Actuators, Shape Memory Alloys, Peltier Devices

This page is intentionally left blank.

Development of Braided Peltier Devices to Achieve Thermoelectric Cooling in Shape Memory Alloy Actuation Mechanisms

Cynthia Xinjia Wang

Supervisor(s): Dr. Johannes Mersch

Abstract— **This dissertation investigates the design and development of braided Peltier devices for achieving active thermoelectric cooling in shape memory alloy (SMA) actuation mechanisms. The research focuses on the integration of periodically nickel-electroplated thermoelectric fibres into flexible braided textile structures that thermally couple and act as a sheath to SMA wires. By leveraging the Peltier effect within the braid architecture, the system is designed to enhance the thermal management and dynamic response of the SMA-based actuators. The work includes fibre fabrication, braid prototyping, electrical and thermal characterisation, and performance testing of the integrated thermoelectric-SMA smart textile. Results indicate that while passive thermoelectric integration modestly improves actuation timing and force response, active Peltier cooling alone was unable to overcome the dominant effects of Joule heating in the current system. Nonetheless, the trends observed suggest potential for improving thermal management in smart textile systems through enhanced thermoelectric design. The findings contribute to the advancement of flexible, textile-integrated thermoelectric devices and their application in wearables and responsive materials.**

Keywords—**Smart Textiles, Thermoelectric Cooling, Braided Actuators, Shape Memory Alloys, Peltier Devices**

I. Introduction

SHAPE memory alloys (SMAs) offer an exceptional combination of compactness, silent operation, and large, controllable deformations, making them highly attractive for wearable actuation. Yet their potential is fundamentally constrained by their thermal cycling speed: while heating for actuation is easily achieved, the rate-limiting step remains the inefficient passive cooling of SMA elements. This limitation caps actuation speed and responsiveness, especially in dynamic or wearable contexts. Thermoelectric cooling presents a compelling solid-state alternative to conventional cooling methods, but prior work has primarily focused on planar, rigid architectures for either cooling or energy harvesting — not on flexible, wearable form factors, and certainly not optimized for SMA systems. Meanwhile, intelligent braided textiles have emerged as a highly promising framework for embedding and protecting functional materials, yet no published work has explored their potential for enabling active thermoelectric cooling within SMA-based wearable actuators.

This thesis presents the first investigation of a braided textile architecture designed to integrate thermoelectric cooling for wearable SMA actuation systems, offering a new approach to address the longstanding cooling bottleneck in these devices.

C. Wang is with the Institute of Textile Machinery and High Performance Material Technology (ITM) at the Dresden University of Technology, Germany. E-mail: cynthia.wang@mailbox.tu-dresden.de .

II. System Design and Fabrication

This thesis developed a novel braided thermoelectric textile sheath designed to provide active cooling for wearable SMA actuators. The system architecture leverages the mechanical flexibility and yarn-level design freedom of braided textiles to realize an integrated Peltier cooling mechanism. To identify a suitable thermocouple material pairing, a wide range of conductive fibres and fine wires were screened via controlled temperature gradient measurements of their Seebeck coefficients. Following prior insights by Hardianto et al. [1], carbon fibre-nickel plated carbon fibre (CF-NiCF) was selected as the optimal combination, offering both adequate thermoelectric performance and compatibility with textile processing.

To support scalable fabrication, a continuous segmented yarn process was developed, combining stencil-based masking with in-line nickel electroplating. A photo of the production process devised by this work is shown in Figure 1. This process enables precise control of electroplating parameters without compromising the yarn length. The final segmented yarn structure ensures reliable formation of CF-NiCF thermocouple junctions when incorporated into the braid.

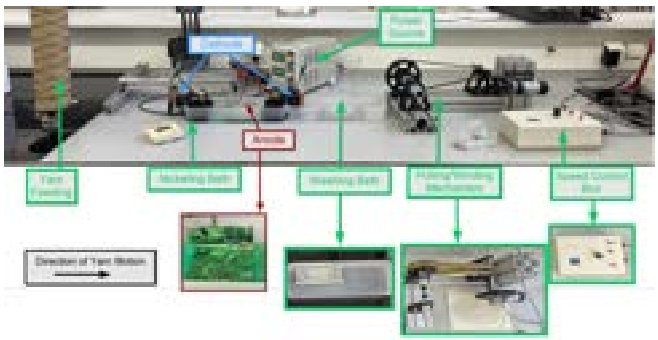

Fig. 1. Image of continuous yarn nickel-plating process

A custom 3D-printed braiding machine was designed and built to produce the target braid architecture. Figure 2 shows the machine during operation, as constructed for this thesis. The design employs four horn gears with six carrier slots per gear, optimized to produce a float length of 3, balancing junction density with manufacturability. TexMind software supported virtual prototyping of the braid structure.

The final device comprises a 7 cm active braided sheath with regularly spaced CF-NiCF segments forming alternating thermocouple junctions on the inner and outer braid surfaces. The

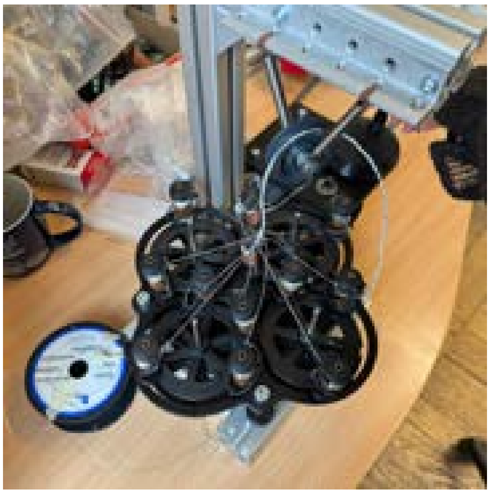

Fig. 2. Braiding machine used for sample fabrication

Fig. 4. Experimental setup for device testing

sheath encases a thermoplastic polyurethane (TPU)-insulated 0.012" (0.3 mm) nickel titanium (NiTi) SMA wire. This configuration potentially enables targeted heat pumping directly at the SMA interface, addressing key limitations of rigid, planar thermoelectric modules for wearable applications. This represents the first demonstration of a fully textile-integrated thermoelectric cooling architecture designed to directly enhance the performance of wearable SMA actuators. A photo of the fabricated device is shown in Figure 3.

Fig. 3. Detail image of fabricated thermoelectric braid

III. Testing and characterisation

To evaluate the impact of the textile-integrated thermoelectric sheath on SMA actuator performance, a series of tests were conducted to measure how active Peltier cooling influences actuation and recovery dynamics. Specifically, the experiments aimed to determine whether heat extraction from the SMA wire via the functional sheath could accelerate the recovery phase after contraction, improving cycle speed and controllability. Mechanical tension, thermal response, and electrical behavior were recorded to assess performance under different heating and cooling conditions.

The experimental setup, shown in Figure 4, enabled precise, synchronized control of both the SMA wire and functional yarn inputs. A FLIR E95 Pro thermal camera captured temperature data, while a 50 N load cell recorded tension response. A programmable power supply controlled both the SMA core and the segmented CF-NiCF sheath independently.

Functional yarn driving currents were optimized to minimize Joule heating while maximizing net cooling. Currents between 0.1 A and 0.3 A were tested, with lower values selected to preserve yarn integrity and maximize thermoelectric efficiency. SMA wires were pretensioned and driven at either 1.6 A for 5 seconds for thermal cycling configurations or 0.5 A for maintaining steady-state contraction.

IV. Results

Four experimental configurations were tested to evaluate the thermal and mechanical performance of a braided textile-integrated Peltier cooling system for SMA actuators:

- Control — SMA heated resistively; passive conductive sheath (no Peltier effect).
- Passive Peltier sheath — SMA heated; Peltier-capable sheath unpowered.
- Peltier-only cycling — Functional yarn driven with alternating polarity; SMA unpowered.
- Peltier cooling — SMA heated; Peltier cooling applied in conjunction to SMA heating.

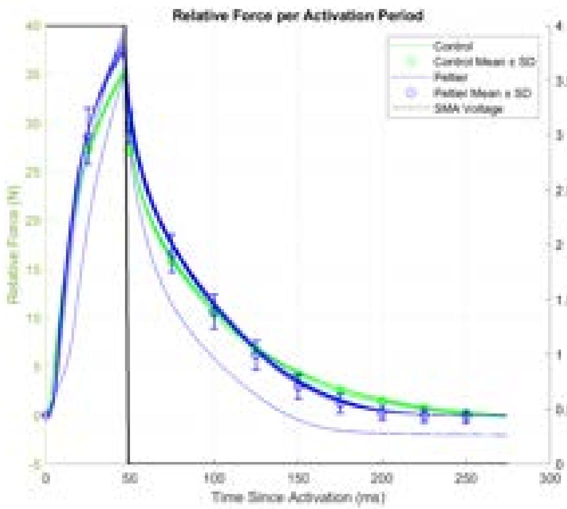

Fig. 5. Comparison of force response for cyclical actuation and cooling for the control and passive Peltier configurations

In the **control vs. passive Peltier configuration** (Figure 5), the thermoelectric braid exhibited a faster rise time and achieved a higher peak actuation force compared to the control, despite the absence of active cooling. Because SMA wire tension is closely correlated with thermal input, the area under the force curve (AUC) was used as a proxy for total heat energy. Results showed that the Peltier-integrated system had a slightly lower AUC on average, suggesting marginally improved thermal efficiency. However, a statistical comparison using a two-sample t-test revealed that the difference was not statistically significant.

Fig. 6. Thermal imagery for Configuration 3: Peltier-only cycling

In the **Peltier-only configuration** (Figure 6), thermographic data showed localized Joule heating within the CF yarn, with temperatures reaching up to $67.4\,^{\circ}\mathrm{C}$ at the braid center. Notably, the metallic crimp regions exhibited faster and higher heat accumulation, highlighting them as major thermal conduction paths that reduce the efficiency of the thermoelectric gradient.

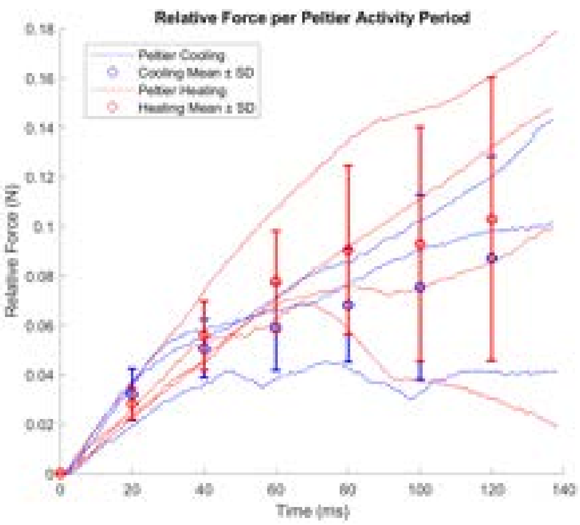

Fig. 7. Comparison of force response during active Peltier heating (red) and cooling (blue) under constant resistive activation of the SMA wire

The **resistive heating with Peltier cooling configuration** shown in Figure 7 applied both SMA activation and active Peltier cooling simultaneously. Although polarity reversal appeared to influence the magnitude of heat flow, the difference in mechanical output between heating and cooling modes was not statistically significant. This suggests that the Peltier cooling effect was insufficient to overcome the dominant influence of Joule heating under the tested conditions.

The discussion identifies several design constraints: (1) parasitic heat loss into the metallic mounting frame and crimps; (2) low Seebeck coefficient of the CF-NiCF thermocouple yarn ($8\,\mu\mathrm{V\,K^{-1}}$); and (3) mechanical instability of thermoelectric junctions under cyclic loading. Opportunities for improvement include using thermally isolating mounting materials, exploring higher-performance thermoelectric yarns, stabilizing junction positions, and integrating metal-based thermocouples for improved performance. While the TE-integrated textile shows promise, overcoming Joule heating and improving thermoelectric material properties are essential next steps for practical implementation.

V. Conclusions

This work demonstrates the feasibility of integrating textile-based Peltier cooling into a shape memory alloy (SMA) actuator system to improve recovery dynamics. A novel braided sheath architecture was developed and systematically tested across several configurations to assess its impact on SMA performance. Initial results suggest that active cooling has the potential to enhance actuator responsiveness, though further refinement of materials and control strategies is needed. Future work will focus on optimizing thermoelectric materials, improving mechanical stability of the sheath, and developing closed-loop control systems to fully realize the benefits of this approach.

Acknowledgments

I thank my thesis supervisor, Dr. Johannes Mersch, for his guidance; Dr. Enrico Sommer for contributions to the fibre experiments; Professor Chokri Cherif and Associate Professor Narantogtokh Davaajav for serving on the assessment committee; and Professor Lieva Van Langenhove and the WE-TEAM programme for shaping my academic perspective. Finally, I wish to thank my family and friends for their support.

References

[1] Anto Hardianto, Benny. Malengier, Gilbert Mey, Lieva Van Langenhove, and Carla Hertleer, "Textile yarn thermocouples for use in fabrics," *Journal of engineered fibers and fabrics*, vol. 14, March 2019.

This page is intentionally left blank.

Table of Contents

List of Figures

List of Tables

This page is intentionally left blank.

List of Acronyms

AUC area under the curve

CF carbon fibre

CNT carbon nanotubes

HCl hydrochloric acid

ITM Institute of Textile Machinery and High Performance Material Technology

NiCF nickel-plated carbon fibre

NiTi nickel-titanium

PEDOT:PSS poly(3,4-ethylenedioxythiophene) polystyrene sulfonate

PBFDO polybenzodifuranedione

SMA shape memory alloy

SMM shape memory material

TE thermoelectric

TEG thermoelectric generator

TPU thermoplastic polyurethane

This page is intentionally left blank.

1

Introduction and literature study

This thesis investigates the development of a novel smart braided textile that functions as a Peltier device for the purpose of active cooling in shape memory alloy (SMA) actuation systems. SMAs are a highly attractive actuation mechanism for wearable devices due to their compact form factor, silent operation, and ability to produce large deformations with simple electrical control. The critical drawback lies in recovery speed: SMAs rely on heating for actuation so the basis of its operation is thermal cycling. The rate at which the material can return to its initial state is fundamentally limited by how efficiently it can release heat. Active cooling is the key to overcoming this bottleneck to unlock faster, more responsive SMA-driven systems.

The contribution of this thesis is to propose and experimentally explore a new textile-based form factor for integrating active thermoelectric (TE) cooling into SMA actuation systems. Prior work on TE textiles has largely focused on energy harvesting or planar cooling applications, and TE-based approaches for SMA cooling remain rare; this leaves a clear gap in the field for a flexible, braided TE textile architecture specifically designed to enhance the performance of SMA actuators. In doing so, it contributes: (1) a novel structural design for textile-integrated TE yarns; (2) a methodology outlining the key material properties, structural requirements, and design principles needed to achieve Peltier cooling for such a device; (3) the design and fabrication of custom lab-scale equipment to prototype such devices; (4) the production and preliminary evaluation of proof-of-concept prototypes; and (5) a critical analysis of the limitations and challenges that must be addressed to make this new category of devices practical.

1.1 Background

In order to provide technical context for this report, this section gives a brief overview of SMA and TE theory. The technical information summarized here is drawn from "Shape-memory Alloys Handbook" by C. Lexcellent [1] and "The CRC Handbook of Thermoelectrics" by D.M. Rowe [2].

1.1.1 Shape memory alloys

Shape memory alloys (SMA) refer to a class of metallic alloys that exhibit a unique, reversible coupling between their thermal and mechanical states, commonly referred to as the shape memory effect. This behavior arises from the presence of a reversible change in microstructure (phase transformation) between austenite and martensite phases. Among this class, nickel-titanium (NiTi) is the most extensively studied and widely used.

To activate shape memory behavior, the alloy must first be annealed: it is held in its desired "memorized" shape and heated to a temperature well above the austenite finish temperature to homogenize and reset the internal microstructure. This is followed by rapid cooling (quenching), which stabilizes the phase distribution and internal stresses. Once "trained", the two phases of interest are the high-temperature austenite phase and the low-temperature martensite phase. Each alloy composition defines a transition temperature for this phase change, which dictates the suitable operating temperature range for which there are dramatic changes in an SMA's mechanical stress-strain behavior. The effects behind SMA operation is further described in Figure 1.1.

When the temperature is above the austenite finish temperature ($T > A_e f$), the material displays **pseudo-elastic** behaviour: stress-induced phase transformation from austenite to martensite occurs during loading, and the reverse transformation occurs upon unloading, resulting in large and recoverable strain, albeit with observable hysteresis. The **shape memory effect** occurs when the temperature

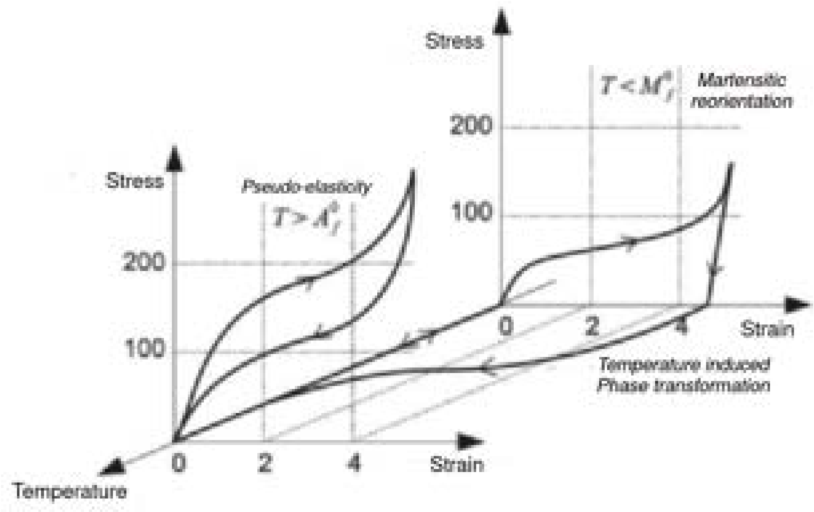

Figure 1.1: Pseudo-elasticity (stress-strain relationship) and shape-memory effect (with temperature change), adapted from Lexcellent [1]

is below the martensite finish temperature ($T < M_e f$). Here, plastic deformation results from the reorientation (detwinning) of martensite under mechanical loading, and retains the strain upon unloading. Subsequent heating above the transition temperature triggers a phase transformation from martensite back to austenite to recover the original undeformed shape. In this process this strain recovery occurs with no change in stress [1]. Together, these effects enable both stress-driven actuation and controllable shape recovery, which form the basis of most SMA actuator designs.

In practical use, the most common method for activating SMA actuators is Joule (also known as resistive) heating, which exploits the material's electrical resistivity to generate heat internally through the application of controlled current. The equation that governs this effect is as follows:

$$Q = I^2Rt \tag{1.1}$$

Here, the generated heat Q is a function of the current through the conductor (I, measured in amperes), the resistance of the material (R, measured in ohms) and the amount of time that the current flows (t, measured in seconds). Joule heating is simple and compact, however theoretically any method that can heat up the alloy to the required temperatures can achieve the same result; activation methods involving lasers and TE heating modules have also been proposed [4]. Joule heating offers no inherent mechanism for active cooling, yet cooling is often the rate-limiting step in SMA actuation cycles. The simplest method is passive air cooling (natural convection), however it is slow and highly variable depending on the environment. For dynamic applications where cycle speed and responsiveness are critical, active cooling methods, e.g. forced air, liquid cooling, or thermoelectric modules are employed to reduce latency and enable higher actuation frequencies. Active cooling methods play a crucial role in overcoming one of the major limitations of SMA actuators and are the driving factor for research and optimization in this field.

1.1.2 Thermoelectric effects

Thermoelectric (TE) effects encompass the direct conversion between thermal and electrical energy in material junctions between two dissimilar conductors. TE theory is comprised of three phenomena: the Seebeck effect, the Peltier effect, and the Thomson effect.

The **Peltier effect** is the basis of TE cooling, and thus it is the primary application of interest in this thesis. It describes the phenomenon in which an electric current passing through the junction surface between two dissimilar conductors causes heat to be either absorbed or released, depending on the direction of current flow. In other words, electrical energy can directly drive thermal transport at the material interface, allowing the junction to function as a solid-state heat pump. This effect enables active cooling of a target region in a phenomenon entirely seperate from convective heat transfer, eliminating the challenge of providing fluid flow. Thus, the field of thermoelectrics are highly attractive for integration into compact and flexible systems such as wearable devices. The **Seebeck effect** is a closely related phenomenon that represents the inverse of the Peltier effect: when a temperature difference exists across a junction between two dissimilar conductors, an electrical current is generated. This is the operating principle behind TE generators, which convert waste heat into electrical power. Finally, the **Thomson effect** describes the generation or absorption of heat when a current flows through a single conductor with a temperature gradient. Although this effect contributes to the overall thermal behaviour of TE systems, it is much smaller in magnitude and thus less frequently exploited in practical device design.

The magnitude of TE efficiency is primarily dependent on the materials' Seebeck coefficient, which is given as microvolts per Kelvin ($\mu V\,K^{-1}$) and represents how effectively a material can convert a temperature difference into an electrical voltage. The Seebeck coefficient depends on the material's electronic structure and can vary depending on factors such as carrier concentration, temperature, and doping. Thermocouple pairs with a large Seebeck coefficient are desirable for both TE cooling and generation, as they result in better efficiency – this will be explained in greater detail later in this section. Experimentally, the relative Seebeck coefficient defined as the ratio between the instantaneous rate of change of the Seebeck electromagnetic force (given in volts) and the instantaneous rate of change of temperature (given in degrees Kelvin) as expressed in the following equation:

$$\alpha = \frac{\Delta V}{\Delta T} \tag{1.2}$$

Applying this theory and excluding all other factors, a Seebeck coefficient of $100\,\mu V\,K^{-1}$ implies a temperature difference of 1 K across the material junction would result in a $100\,\mu V$ difference in electric potential. This is understood to be the result of the Seebeck effect, because this voltage is a result of the thermal difference between the materials. As a result of the Peltier effect, that same Seebeck coefficient also implies that an applied voltage of $100\,\mu V$ in a closed circuit with current flow would cause 1 K worth of heat energy to transfer across the junction. Together, the Peltier and Seebeck effects provide the basis for the development of TE devices that can either pump heat (cooling) or generate electrical energy (power generation). The remainder of this background section will further examine the material properties and device architectures that influence TE performance, with particular emphasis on information relevant for their integration into textile-based systems.

Thermocouple architecture

Thermoelectric (TE) devices are fundamentally composed of thermocouples i.e. pairs of dissimilar semiconductors joined with an electrical contact. A basic thermocouple architecture is illustrated in Figure 1.2. In this idealized representation, a positive-type (p) and a negative-type (n) conductor leg are connected via perfectly conductive materials labeled A, B, and C. The electrical connection for the legs at the top (conductor B) serves as the hot-side contact with temperature T_1 – this is the heat source. The conductors A and C at the bottom are therefore cold-side contacts with temperature T_2 – this is the heat sink. When an electric current passes through this structure, the Peltier effect causes heat to be absorbed at one junction and released at the other, enabling active heat pumping from source to sink across the device. Conversely, when a temperature gradient exists between T_1 and T_2, the Seebeck effect generates an electrical voltage across the circuit, allowing the device to function as a TE generator. The direction of current flow and temperature gradient determine whether the thermocouple operates as a cooler, heater, or generator; reversing the current direction swaps the positions of the heat source and heat sink, and the current direction will also vary depending on whether T_1 or T_2 is at the higher temperature.

Several design considerations strongly influence thermocouple performance. For example, there is a critical tradeoff in the geometric parameters of the conductor legs. Increasing the surface-to-volume ratio i.e. thinner, longer legs offer lower thermal conductivity and reduce heat leakage, however this will also simultaneously increase the electrical resistance leading to greater Joule heating that counteracts the cooling effect. Thus, the geometry and cross-sectional area of the thermocouple legs should also be optimized to balance these competing effects. The following section will further examine material selection considerations that impact TE device performance.

Material properties for thermoelectric performance

The performance of a TE device is strongly dependent on the material properties of the conductors chosen for the thermocouple. This section will discuss the following key parameters: the Seebeck coefficient, thermal conductivity, and electrical resistivity and how they determine the suitability of a given material pair for TE applications.

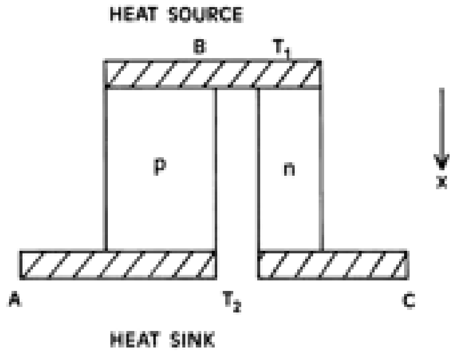

Figure 1.2: Basic thermocouple architecture consisting of positive (p) and negative (n) conductor legs connected between a heat source and a heat sink. Adapted from Rowe [2]

The most direct dependency relationship between a thermocouple and their TE efficiency is through the **Seebeck coefficient**. According to Rowe [2], most metals exhibit Seebeck coefficients of less than $10\,\mu V\,K^{-1}$, which corresponds to a poor TE efficiency of less than 1%. In contrast, suitable TE semiconductors might have Seebeck coefficients in the range of 100-300 $\mu V\,K^{-1}$. It is also important to note that the Seebeck coefficient is temperature-dependent and must be optimized for the intended operating range of the device.

The Seebeck effect is fundamentally an interfacial phenomenon: the source of heat absorption or generation is on the junction surface. In practice, thermal conductivity (measured by $W\,m^{-1}\,K^{-1}$) is a relevant material property to the ability of a material to conduct heat, so it plays a critical role in the behaviour of the surrounding bulk material when considering the system dynamics. Thus, the material bulk should have **low thermal conductivity** to minimize efficiency lost in the form of heat migration away from the desired area in the junction.

Another significant source of inefficiency in TE systems is Joule heating, which occurs when electrical current passes through a material with finite resistance and causes a portion of the electrical energy to be dissipated as heat. Joule heating is a bulk phenomenon that can not only counteract but it frequently overpowers the desired TE effects. To minimize this type of loss and improve overall device performance, it is essential to select conductors with **low electrical resistivity**. However, achieving both low electrical resistivity and low thermal conductivity is inherently challenging, as these properties are often inversely related; materials that conduct heat poorly also tend to conduct electricity poorly. Careful material engineering and doping strategies may be able to optimize this tradeoff and enhance device performance.

To quantitatively evaluate the overall potential of a TE material, researchers may use the dimensionless **figure-of-merit** Z:

$$Z = \frac{(\alpha_p - \alpha_n)^2}{KR} \tag{1.3}$$

where α refers to the seebeck coefficient, K is the thermal conductivity, and R is the electrical resistivity. It is evident from Equation 1.3 that to maximize TE performance, i.e. to maximize Z, would be to increase the seebeck coefficient and minimize the thermal conductivity and electrical resistance.

In addition to these intrinsic material properties, interface effects play a crucial role in thermocouple performance. Contact resistances at the junctions between the semiconductor legs and the metallic connectors (points A, B, and C in Figure 1.2) can significantly degrade efficiency by introducing additional electrical and thermal barriers. To mitigate these losses, careful selection of joint materials and optimization of fabrication processes for all materials in the system are essential.

1.1.3 Thermoelectric devices

Devices capable of converting between thermal and electrical energy are attracting growing interest due to their simple architecture capable of compactness and silent operation. These features make them promising for emerging applications in smart textiles, where integrating TE functionality into fibers and fabrics could unlock new possibilities in wearable thermal management and energy harvesting. To provide context, this section reviews the main types of TE devices and their applications, laying the groundwork for further discussion on smart TE textiles.

Types of thermoelectric devices

Thermoelectric (TE) devices can generally be classified according to which effect (between Seebeck and Peltier) they exploit in their operation. Devices that leverage the Peltier effect are used for active heat pumping, while devices that leverage the Seebeck effect are used for power generation.

A **Peltier device** is a type of TE device that uses the Peltier effect to create a temperature difference when an electrical current is applied. Commercial Peltier modules are comprised of a close array of thermocouples that are electrically connected in series and thermally connected in parallel between two ceramic tiles. When current flows through the module, heat is absorbed on one side (cooling) and released on the other (heating) of the tile. The tile serves as electrical insulation while still being an effective vector for thermal conduction. However, conventional Peltier devices are typically rigid and planar, which is a functional barrier to successful integration into flexible textile systems.

Another widely used category of TE devices is the **thermoelectric generator (TEG)**, which exploits the Seebeck effect to generate electrical power when exposed to a temperature gradient. Interestingly, the underlying materials and architectures that a TEG is comprised of, i.e high Seebeck coefficient, low thermal conductivity, and low electrical resistivity are also the ones that make for an effective Peltier device. The same TE module can function either as a generator or a cooler, depending on whether it is operated under a temperature gradient or an applied electrical current. Thus, in principle, any efficient TEG can also serve as an efficient Peltier device, though highly optimized material devices may favor one mode of operation over the other. For example, Peltier device operation frequently involves higher currents than TEGs, which means that joule heating is a greater concern. Thus, when designing Peltier devices it is more critical that the materials are optimized for low electrical resistance.

Applications of thermoelectric devices

Peltier device and TEG development are the subject of extensive academic research and continued innovation. This section highlights key applications of each device type and the motivations driving ongoing research in these areas.

Solid-state cooling and heating using Peltier devices offer key advantages: Peltier modules are compact, silent, and operate without moving parts or refrigerants, making them highly suitable for applications with space and packaging constraints. An additional advantage of Peltier devices is their ability to seamlessly switch between heating and cooling on the same surface, simply by reversing the polarity of the applied voltage — a feature that is highly attractive for applications requiring reversible thermal control. The most common application of a Peltier device is to cool electronic components (e.g. microprocessors), particularly in situations where it is impractical to implement conventional cooling systems like liquid cooling or forced airflow. As a result, current research in this field prioritizes scaling down Peltier modules to meet the demands of increasingly miniaturized electronic systems. In their 2025 review, Lu et al. hypothesize that future development of Peltier devices will be driven by this ongoing trend toward miniaturized electronic systems, and identify promising approaches in nanotechnology and optimized ultra-thin device architectures [5]. Personal thermal management devices based on Peltier cooling, such as the Embr Wave wristband, are also emerging [6]. These wearable devices use small Peltier elements to provide on-demand localized heating or cooling to enhance personal comfort to the wearer [7]. These devices are gaining popularity in the consumer health market, particularly in applications related to women's health, e.g. managing menopausal hot flashes [8]. Such wearable TE products reflect growing interest in flexible and personalized thermal control systems, and are an area where textile-integrated TE devices could offer significant new opportunities.

The thermoelectric generator (TEG) represents another major application of TE technology, with growing research interest driven by global sustainability goals. Converting waste heat into electrical power is highly attractive, and the Seebeck effect is a promising means of partially recovering the vast thermal energy losses typically present in industrial and transportation sectors. This capability aligns strongly with environmental priorities, as improving waste heat recovery can significantly reduce fuel consumption and greenhouse gas emissions associated with increasing global demand for energy sources like batteries. As highlighted by Duy et al. in their 2025 review, a key motivation for TEG development is the large amount of energy lost in processes such as engine exhaust, industrial furnaces, and power generation, where temperatures reaching up to 600 °C offer significant potential for thermal energy harvesting [9]. However, current TEG performance is limited by low conversion efficiencies, as well as materials challenges related to thermal stability, mechanical durability, and cost. Nevertheless, with rising energy prices, stricter emissions policies, and advances in TE materials and device design, TEGs are expected to continue playing an important role in sustainablity-driven innovations.

1.2 Literature review and state-of-the-art

To contextualize this research and inform the development of an effective design strategy, the following literature review examines three key areas. First, SMA actuators are examined in combination with TE cooling, with a focus on identifying material compatibilities and associated challenges. Second, existing methods for integrating TE functionality into textiles are categorized and analyzed to understand how prior work has approached the challenge of embedding TE devices into wearable formats. Finally, recent advancements in intelligent textiles with braided architectures are reviewed, providing background into the structural characteristics of braiding and its potential advantages for this application. Together, these topics establish the basis for the design rationale behind the innovations explored in this thesis.

1.2.1 Research strategy and query engineering

The literature filtering strategy and supporting text found in Appendix A describing the filtering strategy were developed in collaboration with OpenAI's ChatGPT, a large language model that assisted in synthesizing literature review abstracts and processing relevance-based exclusion filters. All final decisions regarding inclusion or exclusion of literature were made by the author. Proper evaluation of abstracts and full papers was conducted by the author to ensure scholarly rigor and relevance to the thesis topic.

1.2.2 Methods of thermoelectric cooling for shape memory alloy actuators

This section reviews the most significant published efforts to develop thermoelectric (TE) cooling systems for shape memory alloy (SMA) actuators. The narrative is structured to follow the progression of five major research groups that made significant contributions to this field between 1995 and 2009. For each team, the evolution of their system architectures and targeted applications is outlined, highlighting how their respective research trajectories addressed key technical challenges and tradeoffs. In addition, selected independent designs from other groups are interwoven throughout the discussion where they complement or contrast with the approaches of the five primary teams, aiming to provide a holistic understanding why interest in TE-cooled SMA actuators has largely plateaued in recent years, and what technological barriers remain to be addressed.

Review of recent attempts with thermoelectric cooling

Texas A&M University was one of the earliest research groups to systematically investigate TE control of SMA actuators, beginning with theoretical work in 1995 and continuing until 2003. Their initial studies combined theory, computation, and experimental validation, producing a one-dimensional model characterizing heat transfer mechanisms inTE-driven SMA systems under various current densities and cooling conditions [10, 11]. Building on this foundation, subsequent work refined design considerations and examined the thermomechanical coupling effects that govern actuator frequency (potentially achieving actuation frequencies up to 30 Hz with thin 6 µm layers) and stress response to predict the performance of thin-film SMA actuators [12, 13]. Preliminary testing of a compact prototype actuator with this operating principle enabled an empirical assessment of bandwidth, stroke, and power requirements [14]. Reflecting the group's strong connection to aerospace engineering, much of this body of work was explicitly oriented toward space applications, claiming that active TE cooling of SMA elements could enable two-way actuation and vibration isolation in launch systems [15]. The underlying concepts also informed later applications in adaptive rotor blade structures, where TE modules were employed to control SMA blade shape during flight [16].

The French nanoscience research group **FEMTO-ST**, based in Besançon, developed a series of SMA microactuators from 1999 to 2009, pushing miniaturization in their TE-based thermal control strategies. Abadie et al. established a thermal model for TE-driven SMA microactuators and validated it experimentally with millimeter-scale prototypes, proposing SMA wires or thin blades as the active elements [17]. The proposed actuator is in the form of a compact cylindrical module (4 mm diameter, 9 mm length), where two pre-curved NiTi blades are symmetrically mounted between conductive rings and bismuth telluride TE elements. The blades are selectively heated and cooled via Peltier junctions to induce antagonistic bending motions, enabling precise bidirectional actuation. Building on this foundation, the group developed an integrated control system to achieve precise temperature regulation across an operational range from -10 to 90 °C, and claimed an improvement in actuator response time compared to Joule-heated designs [18]. Subsequent modeling efforts focused on predicting the bending behaviour of thin SMA blades to facilitate flexural actuation [19]. The laboratory then translated this research toward practical biomedical applications, stacking multiple actuator modules in series to form articulated structures where each stage contributes an independently controllable degree of freedom for complex, snake-like motion; it was found that this approach was useful for surgical devices used in confined environments like endoscopies [20, 21]. The broader concept of SMA-based microgrippers was further advanced by Jeong et al., who utilized segmental TE control (further discussion of this aspect is provided later in this section) for applications in soft robotics [22]. Finally, Shelyakov et al. pushed miniaturization even further by fabricating TiNiCu (Titanium-Nickel-Copper) SMA ribbons via melt spinning, enabling rapid-response microgrippers capable of handling sub-100 microm objects with Peltier-based thermal control [23].

Tohoku University focused on implantable SMA actuators between 2000 and 2005, tackling the challenge of fully biocompatible constructions. The group first addressed the challenge of precise thermal control by developing a closed-loop controller for SMA actuators employing Peltier modules to improve frequency response for both heating and cooling [24]. Building on this control foundation, Maruyama et al. demonstrated one of the applications of this technology in an artificial heart muscle, where the actuator design consists of SMA coil springs mechanically coupled to a flexible diaphragm and Peltier elements directly attached to the springs. This arrangement enables controlled bidirectional displacement of the diaphragm and achieved a contraction frequency of 1 Hz, which is suitable for cardiac assistance [25, 26]. As the program progressed, efforts shifted toward miniaturization, integrating biomimicry with a baroreflex-inspired feedback system incorporating a ball screw magnetic motor in their artificial myocardium design to enable adaptive cardiac support synchronized to physiological demand [27]. Finally, Luo et al. refined the actuator architecture to further enhance thermal response speeds and expand the operational temperature range of SMA-based manipulators, improving the viability of these devices for dynamic biomedical environments [28].

D'Arbeloff Lab at the Massachusetts Institute of Technology (MIT) developed a "segmented binary control" architecture between 2004 and 2006, where SMA wires were divided into discrete segments whose thermal state (hot or cold) was controlled individually using Peltier modules. Cho and Asada approached this research with a strong emphasis on applications in soft robotics and multi-axis actuation, prioritizing control strategies that enable fine-grained modulation of actuator displacement [29]. The initial prototype demonstrated the feasibility of this approach and laid the foundation for subsequent optimization of control methods to reduce latency and exploit the SMA's hysteresis for improved energy efficiency [30, 31, 32]. Parallel efforts expanded this architecture to two-dimensional arrays [33] consisting of SMA wires arranged in parallel on a PCB substrate, with each wire segmented by localized TE modules that provide bidirectional heating and cooling; by selectively activating combinations of these segments, precise multi-axis displacement patterns can be generated to drive complex robotic motions, such as finger postures in a robotic hand [34]. The team also explored other practical applications, including integration into multifunctional car seats where the same Peltier elements provided both actuation (massage) and thermal comfort for passengers [35]. Further refinement of the system introduced dual-function architectures where TE modules served not only for actuation but also for in-situ temperature sensing via the Seebeck effect, enabling closed-loop control without additional sensors [36]. This architecture has since influenced other segmented SMA actuator designs in wearables, such as Sun et al.'s work on bionic finger joints [37] and Yoong's approach to wrist joints [38]. However, more recent applications of segmented SMA actuators move away from TE cooling, and instead incorporate active fluid coolant, such as Jeong et al.'s designs from 2022 [39].

The most recent (2008-2009) team to develop a TE-cooled SMA actuator system is the **Institute for Technological Research** (IPT) in São Paulo, Brazil, who focused on creating a lightweight, compact actuator architecture suitable for robotics and biomedical applications. The team first developed a comprehensive mathematical model of the proposed SMA actuator system, which incorporated a Peltier-based cooling approach designed to simplify control relative to forced-air or liquid cooling methods. Romano et al.'s actuator consists of a single SMA wire arranged in series with a pulley system, where contraction of the wire—thermally cycled via an adjacent thermoelectric module—rotates the pulley to lift an external load; the resulting displacement is amplified by the pulley ratio and measured using an attached potentiometer for closed-loop control [40, 41]. Building on this foundation, the team implemented a nonlinear sliding-mode controller to enhance stability and faster thermal cycling [42].

Most of the actuator systems reviewed in this section rely primarily on TE-based thermal control, intentionally forgoing Joule heating in order to achieve more precise or localized temperature management. However, the fastest and most responsive SMA actuation systems are likely to combine both methods to leverage the rapid heating that direct electrical current is capable of. A hybrid approach was proposed by Wakasa et al., who developed a control algorithm capable of dynamically coordinating Joule heating and Peltier-based cooling to optimize actuator response time [43]. Their method demonstrated that intelligently combining both mechanisms can significantly improve cycle speed and efficiency, pointing toward a promising future direction for high-performance SMA actuator design.

Pain points and research gaps

While the teams reviewed previously made significant advances in the design of TE activated and cooled SMA actuators, the field has seen limited continuation in the past decade. It is likely that the known limitations of TE modules, namely: low efficiency, heat dissipation, and high power consumption often constrain system performance, particularly for applications requiring large forces or very fast actuation cycles. These hurdles, combined with the rise of competing cooling strategies, shifted research attention away from thermoelectric approaches.

Efficiency – TE modules provide precise, compact, and reversible thermal control; however, their inherent limitations in heat flux density and coefficient of performance (COP) constrain their ability to manage the substantial latent heat demands associated with rapid and cyclic SMA actuation. Several approaches mentioned in the previous section required supplemental thermal management or control workarounds to compensate for the limited heat pumping capacity of the TE modules [11, 18, 26, 32, 42].

Heat dissipation and high-frequency actuation cycles – Prototypes aimed at high-frequency applications frequently encounter bottlenecks due to insufficient cooling rates and thermal saturation within the TE modules. Inadequate heat dissipation not only limits actuation bandwidth but also introduces performance degradation over time. For example: Texas A&M's early models achieved only 2 Hz full cycling due to thermal limits [11]; Tohoku University's artificial myocardium remained constrained to 1 Hz despite incorporating Peltier cooling [26]; the MIT segmented arrays had a large form factor and still required sophisticated hysteresis-based predictive control to mitigate heat buildup across segments [32]; the IPT system used forced airflow to maintain stable operation over extended cycles [42].

Power consumption and scalability – Maintaining large thermal gradients with electrically driven Peltier devices often results in substantial power consumption, significantly reducing overall system efficiency. This challenge is particularly critical for implantable and wearable applications where battery capacity is constrained. Scaling the system to achieve higher actuation forces necessitates increasing the volume of SMA material, which further exacerbates power demands: MIT's 10-axis segmented array required 50 individual Peltier modules [34], illustrating how power draw and system complexity grow disproportionately in designs with multiple degrees-of-freedom. Additionally, achieving reliable and uniform thermal interfaces between SMA elements and TE modules remains non-trivial: both MIT and IPT's prototype reported the need for compromises in thermal contact or supplemental blower cooling to maintain effective operation [34, 42]. As system architectures scale up in requirements, the number of required TE elements, thermal management components, and control channels increases substantially, often leading to diminishing returns in size, weight, and cost.

Another factor contributing to the decline in TE-based SMA actuator research has been the rise of **elastocaloric cooling** as a viable alternative [44]. Elastocaloric systems exploit the latent heat exchanged during stress-induced martensitic transformations within SMA materials themselves, thereby eliminating the need for extra elements such as TE modules. Like TE-based systems, elastocaloric approaches are inherently silent, which is the main advantage for applications such as biomedical implants, wearable devices, and soft robotics. In addition, elastocaloric cooling offers higher potential energy efficiency, more favorable scalability (particularly for micro- and meso-scale actuators), and simpler mechanical integration (since the same mechanical form is used both for actuation and for heat exchange), making them an attractive direction for many researchers in the SMA field.

Given these challenges, it is clear that significant barriers remain to the realization of fully practical, high-performance TE-cooled SMA actuators. However, important opportunities still exist. Recent advances in high-performance TE materials and hybrid control architectures (such as the combination of Joule heating with TE cooling [43]) offer promising pathways to address many of the aforementioned limitations. Additionally, application areas such as wearable robotics, textile-integrated actuators, and biomedical implants place a high value on silent, vibration-free, and reversible controlled actuation, which are still domains where TE approaches show significant potential. Although little new work has been published on TE-cooled SMA actuators in the past decade, parallel advances in related fields, particularly in textile engineering and integration, suggest that there are many opportunities worth revisiting in this area. The remainder of this literature review will explore recent developments in the textile integration of thermoelectric devices and their potential application to wearable form factors.

1.2.3 Methods of textile integration for thermoelectric devices

The integration of TE functionality into textiles is a rapidly evolving field, driven by the demand for energy-harvesting and active cooling systems suitable for textile-based wearables. Numerous approaches have been explored to embed TE materials and architectures into textile structures, each offering varying levels of mechanical flexibility, TE performance, and compatibility with textile processing techniques. The goal of this section is to provide an overview of these integration methods as reported in the literature, and to critically assess their relative effectiveness for applications such as wearable electronics and active cooling. The main strategies identified can be broadly categorized into yarn-based, matrix-based, coating-based, and knitting or embroidery-based approaches, and the papers mentioned in this section are summarized in Table 1.1.

Yarn-based approaches

One of the most promising strategies for creating textile-based TE devices is to incorporate the TE functionality directly into yarns, taking advantage of their inherent flexibility and compatibility with conventional textile manufacturing processes. A common method is to segment the yarn into alternating regions of two different conductors to serve as p-type and n-type sections, creating a series of TE junctions along its length. This segmented structure enables the yarn itself to act as a linear TE generator while remaining flexible and textile-friendly.

Various fabrication techniques have been explored to achieve this architecture. One strategy is to coat alternating sections of the yarn with TE materials before integrating into the textile. Dong et al. [45] and Craighero et al. [46] demonstrated this by dip-coating conductive base yarns (carbon nanotubes (CNT) or polybenzodifuranedione (PBFDO)) with poly(3,4-ethylenedioxythiophene) polystyrene sulfonate (PEDOT:PSS) to form segmented p-type and n-type regions, respectively. Similarly, Kim et al. developed a flexible thermocouple by chemically reducing graphene fibres with a hydrochloric acid (HCl) solution [47], and Yin et al. approached the challenge of developing air-stable n-type CNT yarns by immersing it in an oleylamine/ethanol solution [48]. These approaches yielded all-carbon TE yarns, illustrating the versatility of carbon-based materials in the field of TEs. The TE yarns were subsequently knitted into straps [45] or embroidered into a polyester spacer fabric and electrically connected with silver conductive paste [48], enabling the development of thermal gradients across the width of each respective textile structure to form wearable TEG with multiple p-n couples.

An alternative method selectively electroplates the uncovered sections of a conductive yarn after the yarn is placed into a textile. For example, Hardianto et al. [49] hand-stitched carbon fibre yarns into a polyester fabric template, applied an acrylic dispersion to mask alternating yarn floats, and electroplated the exposed regions with nickel. This produced a linear chain of CF to NiCF thermojunctions integrated directly into the textile. These approaches all face the limitation of finding and using compatible base-yarn/coating pairings so to avoid needing to sever yarns to create physical junctions.

An approach based on physical junctions was demonstrated by He et al. by fabricating core-sheath CNT/PEDOT:PSS nanofibre yarns through continuous electrospinning [50]. These yarns were subsequently connected in series to form a wearable device. However, it is clear that the scalability of this method remains limited, as their prototype wristband incorporated only eight TE junctions. Yang et al. employed a process where an ultraflexible silver(I) selenide (Ag_2Se) and silver (Ag) TE thin film was first fabricated, then cut into equal-length strips. These strips were connected to form a continuous series of electrical junctions, which were then integrated into a knitted structure by tucking the resulting long strip (which is effectively a TE yarn) into the pre-tensioned knit base fabric. The junctions on the strips were carefully aligned with opposite surfaces of the fabrics to follow the direction of vertical heat flux, optimizing the temperature gradient across the device [51].

A persistent challenge in yarn-based TE devices is the development of flexible and oxygen-stable n-type materials. Many high-performing n-type materials are inherently brittle and prone to degradation when exposed to air, making them unsuitable for the mechanical demands of textile applications [46]. Flexibility is especially important in yarn-based approaches, where the yarns must be able to bend and conform through the thickness of a textile to position alternating p- and n-type junctions on opposite fabric surfaces, enabling the formation of a thermal gradient. Without sufficient mechanical compliance, common n-type materials would fracture or lose performance during textile manufacturing processes such as knitting/weaving/embroidery, or during repeated wear. Recent advances, such as wet-spinning polyurethane embedded with MXene nanoflakes to create stretchable fibres [52], or developing air-stable n-type CNT/polymer hybrid yarns [46], represent promising steps toward overcoming these limitations. Overall, yarn-based approaches hold great potential for creating TE textiles, though further progress is needed in materials development to create good thermocouple pairings with high Seebeck coefficients and scalable fabrication techniques.

Matrix-based approaches

Matrix-based approaches aim to produce flexible films by embedding TE materials within a polymer matrix or composite structure. While this strategy does not preserve the ordered fibrous structure of conventional textiles, its flexibility still allows it to be easily integrated into garments or wearable products through methods such as sewing or adhesive bonding. A key benefit of matrix-based films is their straightforward compatibility with nonwoven textiles, which are extensively used in personal protective equipment (PPE), healthcare products, and other industrial applications. An interesting approach by Chen and Lwo involved an electrospinning process that incorporated bismuth telluride powders into polymer fibres, yielding a porous, flexible thin film with promising TE properties [53]. The electrospun films could be deposited on various substrates such as aluminum foil, paper, and Velcro straps, highlighting their versatility and suitability for wearable applications. The previously mentioned yarn-based approach by Yang et al. had an additional hot pressing step after electrospinning their Ag/Ag_2Se solutions to produce a thinner film before cutting into strips to achieve a more compact segmented yarn-like form factor [51]. Although there are challenges apparent with these early approaches, particularly in improving electrical conductivity and power factor, electrospinning presents a fabrication method with great potential for developing TE films that can be integrated with nonwovens.

Coating-based approaches

Coating TE materials directly onto fabrics or yarns allows a high degree of flexibility in processing while largely preserving the inherent structure and properties of the underlying textile. This method typically involves formulating a mixture of TE substances that can be deposited onto the textile substrate and subsequently cured to create a cohesive composite material. Karalis et al. developed a TE paste by incorporating tellurium nanowire powder into a PEDOT:PSS matrix, producing a nanoparticle-based coating. The paste was applied to a glass fibre woven fabric via blade coating, depositing a uniform thin layer on the textile surface. This system demonstrated an exceptionally high Seebeck coefficient of $189\,\mu V\,K^{-1}$ [54]. However, a notable tradeoff in such nanoparticle-polymer composites is that increasing the nanoparticle content tends to reduce electrical conductivity, even as the Seebeck coefficient improves.

Panbude et al. employed a solvothermal method to coat cotton fabrics in situ with a hybrid layer of polyaniline (a conductive polymer) and graphene oxide. Their coating aimed to improve thermal stability (up to $280\,^{\circ}C$), electrical conductivity, and durability. In their 2021 study, the coated fabric achieved a Seebeck coefficient of $85.5\,\mu V\,K^{-1}$, outperforming similar TE coatings based on conductive polymers (e.g., polyaniline, PEDOT:PSS) and carbon materials (e.g., graphene, carbon nanotubes) published through 2012-2018 by at least a factor of two [55]. Furthermore, the coatings exhibited high UV resistance, making them suitable for outdoor applications. However, these coatings were applied to non-stretchable woven textiles. To address the limitations of stretchability, Peng et al. introduced a polydopamine adhesive layer that forms hydrogen bonds with MXene flakes, enabling robust binding to nylon fabrics [56]. This approach resulted in a flexible and stretchable TE coating capable of dual-function sensing (temperature and strain). However, the Seebeck coefficient achieved with this system was lower compared to the previously mentioned coatings. Overall, coating-based approaches offer a versatile pathway for integrating TE functionality into textiles.

Knitting and embroidery-based approaches

Knitting and embroidery-based integration techniques create material junctions through contact by the textile structure itself, offering unique advantages in flexibility and stretchability while maintaining electronic connectivity. This enables the development of wearable TE textiles that can conform to body movement or curved surfaces without significant performance loss.

One approach involves creating stitched junctions, where conductive TE elements are sewn or embroidered onto the textile surface. Several studies have identified sewing coated textiles into functional smart devices as one of the most straightforward fabriction methods. For example, Dona et al. synthesized indium-doped molybdenum disulfide nanosheets directly onto carbon fabric, achieving a Seebeck coefficient of $12.8\,\mu V\,K^{-1}$ [57]. However, scalability remained a challenge, as their prototype contained only four thermocouple legs consisting of fabric strips coated with TE material, that were sewn onto a cotton base fabric using silver-coated thread to achieve electrical connectivity. A more recent attempt by

Farooq et al. adopted a similar sewn-strip approach using graphene-based coatings. In this work, cotton fabric strips were impregnated with a polyvinylidene difluoride (PVDF) and graphene nanoplatelet (GNP) solution, followed by oven drying to remove the solvent [58]. The resulting flexible thermocouples were integrated into a textile-based temperature sensor, highlighting continued progress in wearable TE device fabrication. However, the form factor/size of fabric strips are large and pose as the limiting factor to power density; junctions can only be made as dense as the size of the strips.

Other approaches use a more compact and lightweight strategy by forming the TE junctions directly on the embroidered threads themselves. Radulescu et al. sewed pairs of metallic threads into a fabric, and threads were overlapped at either end of the fabric to create the necessary junctions [59]. This simple and scalable fabrication technique is highly accessible, as it leverages conventional textile processes such as embroidery and sewing which can be easily adapted to a variety of fabric types. While Radulescu et al. employed metallic thread pairings with intrinsically low Seebeck coefficients, the underlying embroidery-based strategy is adaptable and could achieve higher performance with more effective material selections. It is important to note that this configuration is optimized for thermal gradients across the plane of the fabric (width-wise), rather than through its thickness. Thus, it is suitable for a different set of potential application scenarios than the previously mentioned approaches. The key advantage of this sewing-based approach lies in its modularity and compatibility with existing garments, as nearly any finished fabric can be embroidered. However, challenges still remain in ensuring robust and durable electrical contact between the stitched elements and the fabric substrate, as well as maintaining performance under repeated mechanical deformation or laundering.

In contrast, other approaches aim to form intrinsic electronic junctions within the textile structure itself, typically through knitting techniques. Spacer knits and warp-knitted composites can incorporate conductive yarns in such a way that the yarn contacts naturally form the TE junctions. Golla et al. developed a warp-knitted glass fibre-metal composite fabric that integrated over 400 thermocouples per module, representing one of the most junction-dense approaches mentioned in this review. In this design, contact from intertwined yarn loops intrinsic to the knitted structure itself provided repeated conductive contact points between yarns, enabling a Seebeck coefficient of $142\,\mu V\,K^{-1}$ [60]. Knit-in integration offers several key advantages for wearable electronics, including mechanical flexibility, breathability, and the capacity to fabricate large-area TE fabrics with minimal post-processing. However, such approaches also pose material challenges: tighter knit structures require conductive yarns with high bending tolerance to ensure reliable electrical contact, long-term mechanical durability, ande avoiding fracture or delamination of the conductive elements. A practical guideline is to employ yarns that can accommodate a bending radius of at least 2 mm at a bending angle of 180°, in order to maintain compatibility with standard knitting machinery [51]. The knittingapproach addresses one of the bigger practical barriers to wearable manufacturing, which is scalability and production consistency. There is another practical barrier in system design that is often overlooked in academic research yet must be overcome to develop wearable devices that are suitable for commercial use; accommodating diverse physiological features often complicates device performance and in many cases anthropometric considerations are deprioritized in the trade-offs made during device design. Newby et al. demonstrated a modular design using 3D spacer-knitted fabrics, where different thermocouple yarns were knitted into the fabric surface and electronically connected via detachable nickel snaps to form p-n junctions [61]. This approach is particularly advantageous as it enables reconfigurable TE devices that are modular in terms of sensor placement, which is an important feature for wearable applications where optimal device performance is dependent on precise sensor positioning. Together, these advancements in knitting-based intrinsic integration highlight the potential of textile-engineered TE systems to bridge the gap between laboratory prototypes and commercially viable, user-friendly wearable devices.

1.2.4 Methods of intelligent braiding

Braiding is a highly promising textile structure for achieving intelligent functionality in wearable applications. This textile process is defined in which three or more yarns are interlaced diagonally around an axis (defined to be the direction of the longest dimension in the product). Braiding supports the continuous orientation of yarns and introduces opposing directions within the same structure. Braided products can range from linear forms such as ropes and cables, to planar structures (flat braids), tubular braids, and even complex three-dimensional forms. However, it is not just a means of housing functional materials; braid parameters are an active contributor to the performance of the final system. This section provides a brief overview of existing braiding mechanisms and the basic operating principles of industrial braiding machinery, and presents a defensible argument, supported by recent academic literature, for why braiding

Table 1.1: From reviewed literature: summary of thermocouple materials and corresponding reported Seebeck coefficients

Authors	**Materials**	**Seebeck coefficient**
Dong et al. [45]	Multi-walled CNT, PEDOT:PSS	$29\,\mu V\,K^{-1}$, $-35\,\mu V\,K^{-1}$
Craighero et al. [46]	PBFDO, PEDOT:PSS	$-18.8\,\mu V\,K^{-1}$, $17.9\,\mu V\,K^{-1}$
Kim et al. [47]	Graphene	$12.5\,\mu V\,K^{-1}$
Yin et al. [48]	CNT	$-80.48\,\mu V\,K^{-1}$
Hardianto et al. [49]	CF, NiCF	$11.61\,\mu V\,K^{-1}$
He et al. [50]	CNT and PEDOT:PSS	$43\,\mu V\,K^{-1}$
Yang et al. [51]	Ag,Ag_2Se	$90\,\mu V\,K^{-1}$
Li et al. [52]	MXene and polyurethane	$-8.3\,\mu V\,K^{-1}$
Chen and Lwo [53]	Bismuth Telluride	$-10.6\,\mu V\,K^{-1}$
Karalis et al. [54]	CF and epoxy composite	$189\,\mu V\,K^{-1}$
Panbude et al. [55]	Polyanaline and graphene oxide	$85.5\,\mu V\,K^{-1}$
Peng et al. [56]	Polydopamine and MXene	$-9.97\,\mu V\,K^{-1}$
Dona et al. [57]	Indium-doped molybdenum disulfide (MoS_2)	$12.8\,\mu V\,K^{-1}$
Farooq et al. [58]	Polyvinylidene fluoride (PVDF) and graphene	$39\,\mu V\,K^{-1}$
Radulescu et al. [59]	Silver, stainless steel yarns	$2.46\,\mu V\,K^{-1}$
Golla et al. [60]	Constantan and Iron wire	$142\,\mu V\,K^{-1}$
Newby et al. [61]	Alumel and Chromel	$62.79\,\mu V\,K^{-1}$

offers a uniquely adaptable and effective platform for developing intelligent textiles.

Types of braiding mechanisms

In order to provide technical context for this report, this section gives a brief overview of different braiding mechanisms and their structural differences. The technical information summarized here is drawn from Braiding Technology for Textiles by Dr. Yordan Kyosev [62].

The most common braiding mechanism is **maypole braiding**. In industrial machines, the element that moves a yarn is called a carrier, and carriers follow defined tracks (whose motion is driven by horn gears) to interlace yarns into braid structures that can be tubular or flat. A diagram of a tubular braiding machine configuration is shown in Figure 1.3, where a carrier slot that contains a yarn is denoted with a dot in the horn gear. An even number of yarn carriers circulate in two opposing directions along two intertwined tracks: one track is defined by the pathway through all the clockwise-turning horn gears, and the other pathway is through the counter-clockwise-turning ones. This type of braiding (also referred to as circular braiding) is the dominant technique in the industry. The circular motion of the carriers creates a tubular structure. The braid angle is the primary geometric parameter in braiding and is defined by the ratio of carrier rotation to take-up speed. Visually, it affects the angle between the yarns and the axis, and is usually between 30°-80°. Maintaining proper yarn tension to compensate for variable yarn path length is managed by mechanisms within each carrier. Circular braiding enables both the production of braids over a core yarn as well as freestanding tubular braids. In flat braiding, the horn gears are arranged linearly and the number of carriers can be even or odd. The carriers follow a closed track and reverse direction at the boundaries, resulting in a flat, tape-like braid. While the motion principle remains similar to tubular braiding, the geometry of the yarn paths differs.

In addition to standard circular and flat configurations, a number of specialized variations on the maypole braiding machine have been developed to expand control over yarn paths and braid geometry. These adaptations demonstrate that the design space of braid structures remains far from fully explored, offering exciting opportunities to engineer novel textile functionalities. A few notable examples are highlighted as follows:

- In **triaxial braiding**, inlay yarns are incorporated along the braid axis, which allow for the insertion of inlay yarns that run parallel to the axis. The axial inlay yarns can be used to add specific functional properties to the braid—for example, adding elastomeric inlays can allow the braid to contract or scrunch.
- **Form braiding** enables the creation of braids with more complicated cross-sections. This is achieved by adding additional tracks beyond the two-track structure of classical maypole braiding, allowing the carriers to move in multiple directions and producing three-dimensional braid

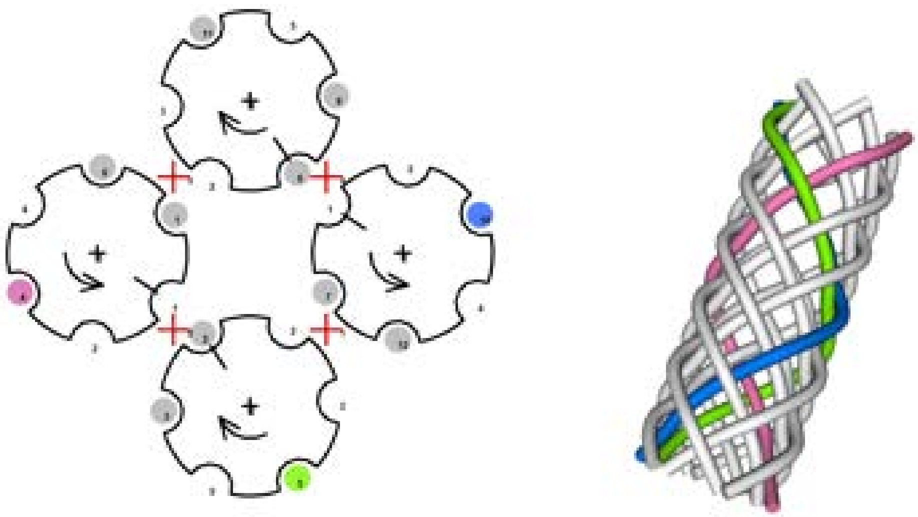

(a) Configuration of 4 horn gears with 6 carrier slots each

(b) Rendered braid with 12 yarns and float length 3

Figure 1.3: Braiding machine configuration, generated using TexMind Braider [3]

architectures. Hexagonal horn gear arrangements are the most interesting recent development in form braiding, as they enable dense packing of carriers and therefore a greater flexibility in cross-section geometry [63]. The addition of digitally controlled cams and switching devices allows dynamic reconfiguration of carrier motion during braiding, enabling highly programmable 3D structures [64, 63] and can even achieve asymmetry along the axis, enabling novel actuation and sensing architectures in smart braids [65].

While a wide variety of braiding mechanisms exist, tubular maypole braiding remains the most common industrial technique and is used as the baseline architecture throughout this report. Unless otherwise noted, the following sections will refer primarily to tubular maypole braided structures.

Braid parameters as opportunities for intelligent textile functionality

The braided textile structure offers a uniquely advantageous platform for intelligent and wearable applications. Braid parameters such as braid angle, yarn tension, yarn diameter, and yarn stiffness can be precisely engineered and tuned to improve control over a wide range of textile behaviours. In addition to this tunability, braiding inherently enhances the mechanical protection and durability of embedded smart materials, which often suffer from low tensile strength and poor abrasion resistance. This makes braiding particularly well suited for compact, comfortable, and efficient electrical integration methods into wearable devices. This combination of mechanical robustness and versatility makes braiding an ideal framework for developing intelligent textile technologies. In this section, we examine specific braid parameters and highlight recent literature examples that demonstrate their potential for enabling novel textile functionalities.

Braid angle is the angle at which yarns are interlaced around the axis of a braided structure and is a design parameter that can directly influence the mechanical response, sensor performance, and actuation behaviour of braided smart textiles. It is generally understood that larger braid angles are correlated with increased stiffness. Beyond modifying stiffness, the braid angle can also influence internal compressive behaviour. In practical applications, Duan et al. employed braided sleeves to encase soft, deformable energy-harvesting materials and found that strain applied to the system was amplified due to radial squeezing effects of the helical yarns in the braid [66]. The study's kinematic modeling and experimental validation confirmed that adjusting the braid angle directly modifies this signal-amplifying effect, which improved the sensitivity of stretchable, gel-based sensors. However, this effect is not singularly relevant for this type of braided device; Qi et al. and Yang et al. also found a critical relationship between braid angle and device functionality in shape memory material (SMM) braids. Their findings showed that braid angles affect both the magnitude and speed of shape recovery, with higher angles generating greater recovery force and lower angles reaching thermal activation thresholds faster [67, 68]. In strain sensors made from braided conductive fibres, Mersch et al. demonstrated the trade-off relationship that higher braid density and braid angle reduce sensitivity but improve mechanical compliance and linearity [69]. In artificial muscle systems, where a a sheath is braided over an elastic hydraulic tube core, it is demonstrated that the braid angle had the strongest influence on contraction force among all tested manufacturing variables (including fibre sleeve material and inner rubber tube thickness) [70]. In an optical sensing system, how strain, bending, and torsion are transmitted to embedded fibres is also critical to sensor functionality. Lee et al. developed a braided fabrication method for optical fibre Bragg grating sensors and found that braid angle significantly impacted strain sensitivity and signal fidelity [71]. These results suggest that engineering braid configurations can optimize mechanical-electrical transduction in a wide variety of textile-integrated sensors.

Asymmetry in braid structures provides structural versatility that has numerous applications in smart textiles. Unequal yarn tensions during braiding result in twist and spiral effects. This built-in twist can also be implemented with water-soluble fibres by dissolving certain fibres after braiding. The resulting twist is dependent on the original braid angle and direction, and this technique was successfully implemented by Tian et al. to produce asymmetrical forces in an artificial muscle [72]. Insights from biomimicry reveal that the plant kingdom has long utilized this principle in their net-like natural fibre networks. Masselter et al. investigated upright growth in plant stems to find that asymmetric fibre angles enable directional bending and structural reinforcement, inspiring the design of actuators whose deformation behaviour (i.e. shortening and thickening versus lengthening and thinning) can be controlled by setting the braid angle above or below the critical angle of 54.7° [73]. Programmable asymmetry is highly desirable, especially when it can result in auxetic behaviour, i.e. negative Poisson's ratio where the material expands laterally when stretched. McAfee et al. showed that geometrical incompatibilities introduced through braid angle (and thus helical yarn wrap angle) variation can induce an auxetic effect [74]. Enhanced energy absorption and improved impact resistance from auxetic textiles have numerous practical applications in personal protective equipment and defense. As such, braid angle is not merely a structural detail, but a key design variable that enables intelligent responses in braided textiles. By controlling braid angle, designers can precisely tune a range of physical properties including stiffness, compression, energy absorption, and strain transmission.

Yarn properties like diameter and stiffness also play a role in defining the mechanical and functional performance of braids because of the dynamic fibre interactions that distribute load through individual yarns. Hoque et al. [75] systematically studied how yarn stiffness and yarn diameter influence the deformation strain and actuation force in an artificial muscle system with a braided sheath over an elastic pneumatic tube core, generally finding the pattern that softer yarns and smaller diameters contribute to greater compliance, enabling higher strain responses under pressure. Conversely, increased yarn stiffness reduces the actuator's ability to deform but increases the actuator force, demonstrating a trade-off between mechanical strength and flexibility. The integration of elastomers into a braided system can offer an additional pathway to adjust mechanical behaviour, as the Young's modulus of the elastomer can affect its bending and force characteristics. Lower modulus materials exhibit greater bending angles and higher blocked forces under the same pressure due to increased radial expansion and axial contraction. In contrast, higher modulus materials resist deformation, resulting in reduced bending and lower force output as demonstrated by Kandasamy et al. and Wu et al. [76, 77]. Remarkably, braiding can also moderate the stiffness of otherwise rigid materials. Dong et al. demonstrated that stiff metal filaments, which are typically unsuitable for wearable applications, are more flexible when braided due to friction and controlled slippage between interlaced fibres [78]. Because braided structures are fundamentally composed of interlaced yarns, even small changes in individual yarn properties can cascade into significant changes in the overall braid properties. Thus, yarn selection is shown to be a critical design decision for achieving targeted outcomes in smart applications.

Braiding textile design strategies for practical wearables

In addition to their ability to tune intelligent textile functionality, there are several textile design strategies unique to braiding that offer an ability to address practical design requirements for wearable systems. Attributes such as durability, comfort, washability, and reliable electrical integration are critical for the successful adoption of smart textiles in real-world applications. The following section highlights several of these key requirements and presents recent examples from the literature that demonstrate how braiding is used to resolve these practical challenges.

Durability is often a challenge with smart textiles as many applications involve repeated strain and many smart materials are mechanically weak. When braiding acts as a reinforcing sheath around a functional core material, tensile strength and fatigue resistance are improved [79] while still maintaining good sensor sensitivity [80]. It has already been mentioned that the braided sleeve in Duan et al. [66] reinforced a soft hydrogel core; this design decision had the additional benefit of added mechanical strength while preserving flexibility. Wang et al. also leveraged this principle in a smart actuator system. By braiding actuation and triggering yarns together in a configuration such that they were constantly touching, the structure of the braid improved tensile strength in otherwise fragile liquid crystal elastomer fibres while also enabling sustained deformation under joule heating stimulation [81]. However, as Madheswaran et al. note, braiding is not universally compatible with all fibre types: extremely delicate or nanofibrous materials can be damaged by the tension and friction that is required during the braiding process [82]. Thus, while braiding is an effective strategy for increasing the durability of smart textiles, its applicability must be balanced against the fragility of the materials being integrated.

Comfort and washability are also important features for practical wearable systems that braiding can help achieve. Braiding can serve as a soft sheath which is an especially useful technique when incorporating materials that are typically rigid, abrasive, or thermally uncomfortable – all without compromising function. An example of a commonly used yet frequently intrusive element is LEDs, where direct skin contact can be problematic due to its usual rigid form factor and heat emission during operation. However, these challenges are mitigated when diodes are braided into e-yarns so they can be easily integrated into fabric without compromising on the function of the light [83]. Washability is also a concern for everyday wearables; Yang et al. [84] showed that incorporating braided insulating fibres around carbon nanotube assemblies significantly improved the durability of textile-based capacitive sensors through multiple wash cycles, without degrading their electrical or mechanical performance. These examples illustrate how braiding can enhance real-world practicality in wearable technology.

Integrated electrical functionality is also something that braiding offers unique structural advantages for. Most approaches either incorporate one or more functionalized yarns into the sheath by wrapping helically around the core [85], or incorporate the functional yarn directly in the core to achieve distributed sensing or actuation. In this section, it has been previously established that braided structures are mechanically robust without compromising on flexibility and can both protect electrodes and allow the electrode fibres themselves to act as active sensing elements. In braids, electrical junctions can accommodate a degree of stretching without electrical failure, a crucial characteristic to enabling reliable performance in soft, deformable systems. These junctions can be continuous along the electrode, completely isolated, or discretely patterned along the braid's sheath, giving engineers control over electrical connectivity within the textile. Several braided sensors leveraged the property where the structure allows different functional fibres: reference, counter, and sensing electrodes to be arranged in controlled proximity in their approaches to strain sensors, moisture sensors, and pressure sensors [69, 86]. Gong et al. [87] treated the braided structure as a programmable matrix, using it to distribute pressure-sensitive capacitive sensing points throughout the textile and enable positional sensing. By tuning braiding parameters such as angle and length, they developed a multifunctional sensor simultaneously capable of flame retardancy, position detection, and high-temperature alarm – all integrated within a single compact axial structure.

Another way to maintain uniform electrode spacing is with multilayered coaxial braiding. Many piezoelectric yarns for practical health monitoring applications utilize multilayered braids, with an inner electrode–piezoelectric layer–outer electrode structure [88, 89]. Concentric layers of braids have also been shown to improve linearity and reduce hysteresis in pressure sensors, as exemplified by Liu et al. in their positionally aware pressure sensor fabricated from a double-braided structure of NiTi shape memory alloys [90]. This demonstrates that coaxial braiding can serve not only to structure electrodes, but also as a powerful means of tuning the performance of functional yarns. Although this fabrication method involves multiple steps, coaxial braids enable more sophisticated electrode layout designs while preserving the key advantages of functional yarns: enhanced comfort and a fully fibre-based construction compatible with standard textile processing.

There are a variety of processes that braided cords can be seamlessly incorporated into larger textile systems. For example, they can be directly sewn onto fabric substrates [91], introduced as weft yarns on weaving looms through pick insertion [92], or incorporated as inlay yarns within knitted fabrics using flat knitting machines [45]. When embedded within composite materials, the braided structure enhances interfacial adhesion with the matrix and enables integrated sensing within the composite [88, 93].

Across these examples, it is clear that the structural characteristics of braiding — its controlled axial and radial fibre positioning, its ability to mechanically stabilize delicate functional yarns, and its capacity to define periodic electrical contact patterns — are highly advantageous and reinforce braiding's potential as a framework for the next generation of wearable and intelligent textile technologies.

1.3 Thesis objectives

While textile-integrated TE systems have been extensively explored for applications such as thermal energy harvesting and wearable cooling [46, 51], and braided smart textiles have been demonstrated for sensing, actuation, and structural applications [75, 87], no published studies to date have combined these techniques to achieve localized active cooling of shape memory alloys. This represents a novel and promising design space that this thesis aims to explore.

The objective of this thesis is to investigate whether a braided textile architecture can serve as an effective and practical form factor for integrating TE-based active cooling into wearable SMA actuation systems. The design approach is intentionally product-driven: rather than beginning from the known limitations of existing TE modules or SMA devices, the project begins by conceptualizing an ideal wearable form factor and then works backwards to prototype a textile structure that could realize this vision. The goal is to identify how braiding — through its inherent mechanical flexibility, tunable structural properties, and compatibility with functional yarn integration — can address key challenges in TE-cooled SMA actuation: achieving effective thermal coupling, maintaining wearable comfort, and enabling scalable and manufacturable designs.

It is fully acknowledged that the prototypes developed in this thesis may not yet achieve full functional parity with rigid TE-cooled SMA actuators. Rather, this work is framed as an initial proof of concept and exploratory study, intended to open a new design pathway for future research. By adopting this product-first perspective, this thesis contributes a novel structural design concept, a prototype fabrication methodology, and a critical analysis of the unique opportunities and challenges presented by combining braiding with TE cooling for wearable SMA actuation systems.

2

System design and fabrication

This chapter presents the complete design and fabrication process of the textile-integrated thermoelectric actuator device, including material selection, functional yarn development, braid architecture design, custom braiding machine construction, and final device assembly.

2.1 Thermocouple material exploration

In a study by Hardianto et al. [94], the authors explored various combinations of conductive textile yarns and metal wires to identify materials suitable for flexible thermocouples and, by extension, integrated into textile structures. Their motivation was to overcome the limitations of metal-wire-based thermocouples, which reduce textile flexibility, and instead identify yarn-based solutions that retain textile feel and processability. They tested a selection of commercial conductive yarns and wires by measuring the Seebeck coefficient of different material pairings under controlled thermal gradients. In this thesis, a similar material screening approach was carried out for the materials available at the Institute of Textile Machinery and High Performance Material Technology (ITM), Technical University of Dresden. Based on these results, one material combination will be selected for use in the textile-integrated thermoelectric device developed in this work.

2.1.1 Materials tested

A wide selection of conductive fibres and wires available at the ITM were assembled for testing. These included both materials similar to those studied by Hardianto et al. [94] and additional materials not previously explored. The Seebeck coefficient was measured for all possible pairwise combinations to evaluate their suitability for textile-integrated thermocouples. Table 2.1 provides an overview of all the fibres and wires used in the tests, along with their manufacturers. A detail image of all the tested materials is shown in Figure 2.1, taken using the TOMLOV DM602 Pro digital microscope.

Table 2.1: Materials tested for Seebeck coefficient: legend and specifications

Short Code	Material	Manufacturer and Make
A	Fe Wire 0.015 mm	J. S. Feindrahtzug GmbH
B	Stainless Steel wire	J. S. Feindrahtzug GmbH
C	Cn wire 0.12 mm	ELEKTRISOLA Dr GerdSchildbach GmbH
D	Cu wire 0.07 mm	ELEKTRISOLA Dr GerdSchildbach GmbH
E	Conductive alloy wire 0.07 mm	Elschukom
F	Steel-plated Fibre	Amann Group Steel-Tech
G	Ag-plated Fibre	Madeira Garnfabrik HC12
H	CF Fibre	Toho Tenax Co., Ltd. HTA40 H15 1K
I	NiCf Fibre (No Sizing)	Toho Tenax Co., Ltd.
J	NiCF Fibre (Sized with Acetone)	Toho Tenax Co., Ltd.
K	Cu/CF Fibre	Inca-fiber

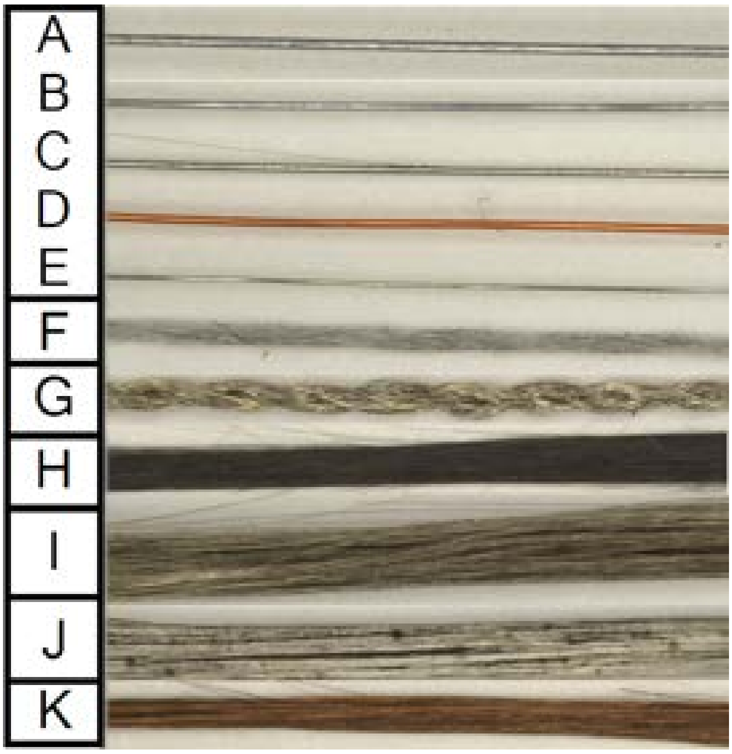

Figure 2.1: Detail images of tested fibres for Seebeck coefficient

2.1.2 Determining the Seebeck coefficients

To ensure consistency and comparability of results, the following procedure was used to measure the Seebeck coefficient of each material pairing. The equipment used for this procedure was a PR 5 SR Hot Plate with Program Controller, and a Fluke 8846A 6.5 Digit Precision multimeter. The full setup is shown in Figure 2.2.

1. The hot plate was pre-heated to 60 °C for one hour, with a 0.5 kg steel weight placed on top to ensure uniform heating across the plate and weight. To electrically isolate the conductors from the metallic surface of the hot plate, a paper cover was placed on the hot plate. The temperature uniformity of the weight was verified with an infrared thermal camera.

2. Each thermocouple material was prepared by folding a piece of masking tape with a small hole cut into it over the conductor. This secured the conductor in place while leaving an exposed section where the junction would be. The sticky region around the exposed section ensured firm, consistent contact with the hot plate when the two conductors are pressed together. A detailed image of the junction is shown in Figure 2.3.

3. The conductors were trimmed to equal length, and the multimeter leads were attached at points exactly 20 cm from the thermocouple junction.

4. The prepared junction was placed onto the hot plate, and the 0.5 kg weight was repositioned on top to ensure stable contact during measurement.

5. After allowing the junction to heat for 20 seconds, the generated voltage (in millivolts) was manually recorded in a spreadsheet.

6. The temperature difference ΔT in Equation 1.2 was calculated as the difference between the hot plate surface temperature and the ambient room temperature, and is also manually recorded in a spreadsheet.

This procedure was repeated for all possible pairs of materials (full list provided in Table 2.1), and the resulting Seebeck coefficients are summarized in Table 2.2. In this table, darker shades of green highlight material combinations with higher measured Seebeck coefficients, providing a quick visual reference for

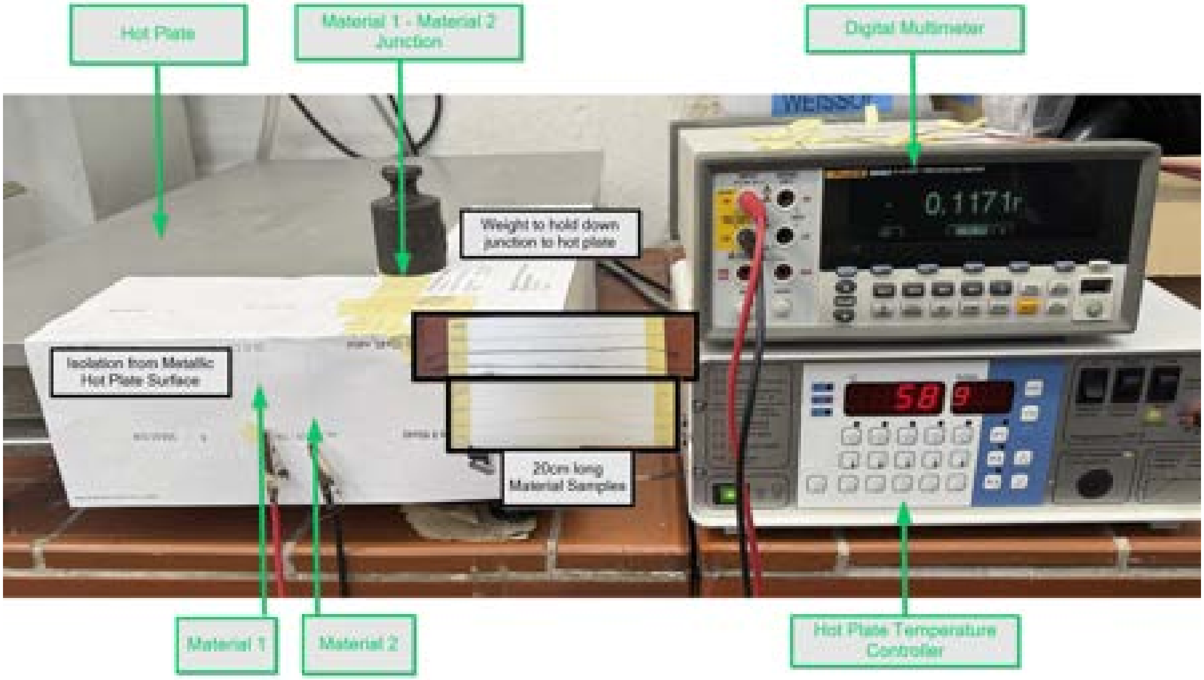

Figure 2.2: Experimental setup for Seebeck coefficient measurement of material combinations

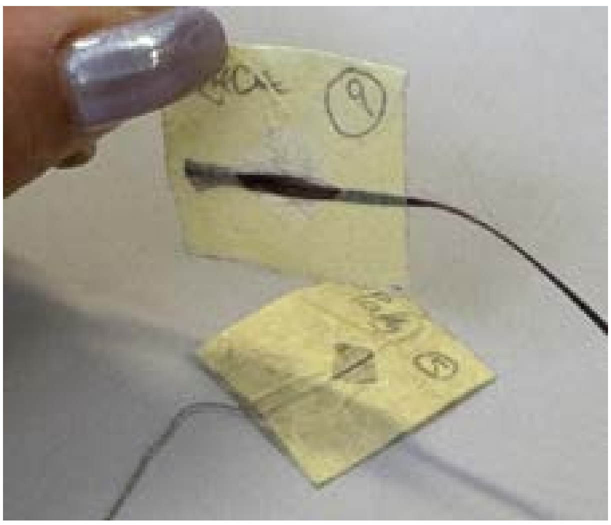

Figure 2.3: Image of simulated thermocouple junction used in Seebeck coefficient testing

Table 2.2: Measured Seebeck coefficients for all material combinations tested

Material Code	A	B	C	D	E	F	G	H	I	J	K
A		4.86	41.14	8.86	7.71	10.29	8.00	10.86	18.29	15.14	7.71
B			41.71	3.57	1.00	4.83	3.14	6.86	12.00	12.29	3.43
C				37.71	36.57	33.43	35.71	32.00	26.86	26.86	34.00
D					1.14	2.57	0.57	2.29	10.29	6.86	0.29
E						4.00	0.71	4.29	10.00	11.14	0.86
F							2.86	0.29	6.86	6.86	2.86
G								2.86	10.57	9.43	0.57
H									5.71	8.00	2.86
I										3.14	7.14
J											7.71
K											

identifying the most promising pairs. Materials A-E in this study are thin-gauge metallic wires, while materials F-K are fibres or yarn-based conductors. This is an important distinction because the physical form factor of the conductors influences how easily different materials can be paired, processed, and integrated into textile structures; this challenge was also discussed by Hardianto et al. [94]. In practical terms, fibres tend to be more compatible with textile processes such as weaving, knitting, or embroidery, while fine wires can pose difficulties in handling and durability.

Several trends emerge clearly from the results. Material C (Constantan wire) consistently produces high Seebeck coefficients in almost every combination, confirming it as a strong performer and versatile pairing material. Additionally, combinations between wires and fibres (seen in the upper right of the table) often yield relatively high Seebeck values, suggesting that hybrid wire-fibre thermocouples could be particularly effective. Another observation is that fibre-fibre combinations (lower right corner of the table) generally yield lower coefficients than wire-wire or wire-fibre pairs, though certain fibre combinations (e.g., involving material H or I) show promise and could be prioritised for textile applications due to their better mechanical compatibility.

Table 2.3 compares the Seebeck measurements of several material combinations that this work and the study by Hardianto et al. have in common. It should also be noted that in cases where multiple variants of the same material were available (for example, two NiCF options in this work, or multiple CF yarns in Hardianto et al.), the higher-performing pairing was selected for inclusion in the comparison table, in order to represent the best-case result for each combination. In general, the same trends observed by Hardianto et al. were reproduced here, as the material combinations follow the same overall ranking from highest to lowest Seebeck coefficient. However, the absolute values measured in this work are typically lower than those reported by Hardianto et al., and in some cases are even more than $10\,\mu V\,K^{-1}$ lower. Several factors could explain these discrepancies. Differences in experimental setup may introduce variability; the temperature difference between the hot plate and ambient conditions was not specified in Hardianto et al., and it is known that Seebeck coefficients can vary depending on the temperature range the thermocouple is subject to. Additionally, material sourcing may play a role: for the CF-NiCF combination in particular, it is likely that different CF manufacturers or differences in surface treatment lead to variations in electrical properties and hence the Seebeck coefficient. This type of variability in carbon-based materials was also noted by Hardianto et al. in their discussion of textile thermocouples [94]. Overall, despite some differences in absolute values, the relative trends between material pairings remain consistent with those reported in the literature, supporting the validity of the material screening conducted here.

2.1.3 Choosing the thermocouple materials

The thermocouple material combination selected for further development in this work is the same as that chosen by Hardianto et al. [94] — a pairing of CF and NiCF. The reasoning is also largely similar. As discussed in Hardianto et al., although the CF-NiCF combination does not exhibit the highest Seebeck coefficient among all tested pairings, within the subgroup of fibre-fibre pairings (materials F-K in Table 2.1), the CF-NiCF combination ranks among the better-performing options. It has been previously established that fibre-fibre pairs offer significant practical advantages for manufacturability and are

Table 2.3: Comparison of Seebeck coefficient results: current work vs. Hardianto et al.

Material Combination	**Code**	**Hardianto et al. [94]**	**This work**	**Difference**
Steel and Cn	B, C	50.78	41.71	-9.07
Cn and Cu	C, D	41.39	37.71	-3.68
Steel and NiCF	B, I/J	25.58	12.29	-13.29
CF and NiCF	H, I/J	19.22	8.00	-11.22
Steel and CF	B, H	5.16	6.86	1.70
Steel and Cu	B, D	1.09	3.57	2.48

highly compatible for integration into flexible textile structures, i.e., the process to create a segmented thermoelectric yarn structure with this thermocouple pairing is straightforward with clear potential for process scaling. Thus, this thesis further proposes to develop a continuous and scalable electroplating workflow specifically tailored to a yarn with CF-NiCF thermocouple pairs.

2.2 Functionalized yarn

This section outlines the development and fabrication processes employed to produce functionalized Ni-NiCF yarn in a novel continuous electroplating workflow. The following subsections detail the methodological choices, experimentation, and resulting techniques that enable the fabrication of segmented, functional yarn suitable for integration into smart textile structures.

2.2.1 Process development for segmented CF-NiCF yarn production

As outlined in Section 1.2.3, previous approaches to producing segmented Ni-NiCF yarn have typically involved a batch-based process. In one method, finite lengths of CF yarn were wound around a template, a conductive silver ink trace was applied halfway width-wise on the template to mark the intended junction location, and subsequently, the template was partially immersed in an electroplating bath so that alternating sections of the yarn were plated with nickel. While this technique does successfully result in the formation of discrete segments along the yarn, it produces limited lengths of functionalized yarn per batch. Furthermore, this method presents significant challenges in terms of scalability, particularly for future applications that may demand continuous or large-scale manufacturing.

Another previously explored strategy involves first incorporating the yarn directly into a textile substrate, followed by selective masking of the exposed regions prior to electroplating. This approach offers precise control over junction placement, enabling alignment with the textile architecture (e.g., alternating sides of a fabric). However, this method is difficult to implement for fine-scale or miniaturized structures, limiting its applicability in scenarios requiring high resolution or smaller yarn diameters. Thus, to enable flexible production, this thesis adopts a different approach: segmenting, masking, and electroplating the yarn prior to its insertion into a textile structure.

To overcome the constraints of batch-based processing, it is also necessary to decouple the masking and electroplating steps, allowing each to be performed independently and incrementally along the length of the yarn. The masking process must be capable of continuously applying precise, spatially controlled insulating regions along an unbroken yarn, while the electroplating process must be designed to plate exposed segments without requiring the entire yarn to be processed as a discrete unit. Achieving this separation is essential to enabling a continuous manufacturing workflow suitable for the scalable production of segmented functionalized yarns.

Approaches to masking fluid

Previous attempts at selective masking for electroplating yarns have employed polymer or acrylic dispersions that require a curing step, typically through air drying, heat, or ultraviolet (UV) exposure, to form cross-linked insulating layers. However, such methods introduce additional complexity and often necessitate access to specialized materials and equipment that were not readily available for this work. Consequently, an alternative strategy was pursued, focusing on identifying simple, off-the-shelf substances that could meet the functional requirements for masking.

As previously discussed, developing a continuous electroplating process necessitates a masking strategy capable of being applied incrementally along the yarn, such that the entire yarn length may be passed through an electrolyte solution. OpenAI tools assisted in brainstorming potential commercially available products that were capable of adhering closely to fibrous surfaces while providing effective electrical insulation and mechanical flexibility. This work devised the following criteria for the masking material:

- It should provide robust electrical insulation to prevent nickel deposition in masked regions.
- It should exhibit high visual contrast relative to the unmasked yarn to facilitate accurate identification of junction locations.
- The masking material should remain securely adhered to the yarn throughout the electroplating process.
- It should not significantly alter the mechanical properties of the yarn e.g. tensile strength, flexibility, or diameter to ensure compatibility with subsequent textile fabrication steps.

A range of candidate materials was evaluated based on these criteria. The substances tested included: paint varnish, white glue (polyvinyl acetate), specialty masking fluid designed for fine art applications, several brands and types of correction fluid, and electronic masking tape. For each candidate, coatings were applied to sections of CF yarn and systematically assessed for:

1. Coating precision and flow behaviour (i.e., ability to remain localized and avoid undesired propagation along fibres),
2. Visibility upon drying,
3. Mechanical stability (i.e., resistance to flaking or brittleness),
4. Impact on yarn handling (e.g., stickiness, stiffness, strength), and
5. Electrical insulation performance, verified using electrical continuity testing on a multimeter.

Through this process, the most effective masking formulation was determined to be a 1:1 mixture of UHU brand water-based correction fluid (selected for its high opacity, flexibility, and rapid drying characteristics) and a generic paint varnish (which contributed greater viscosity, improved electrical isolation, and enhanced elasticity). This combination yielded a masking layer that adhered securely to the yarn, resisted mechanical degradation during electroplating, and maintained excellent electrical isolation performance.

Approaches to segmented masking

Several approaches were explored to develop a method for applying precisely segmented masking patterns along the length of the yarn. The goal was to identify a scalable, consistent process that could produce high-quality masks suitable for use in continuous electroplating.

Several preliminary approaches were explored to identify the optimal masking technique, although they ultimately proved impractical or excessively complex. Briefly outlined here are two notable examples that informed the selection of the final masking method. An initial approach utilizing gear-driven rollers with foam-covered spur segments was abandoned due to difficulties achieving uniform coatings and impractical mechanical complexity. A second approach involved winding yarn helically around a cylindrical template, which was designed to accept snap-in gaskets that would create recessed grooves for the masking fluid. This proved to be unfeasible too due to fabrication constraints, fragility of the printed parts, and excessive masking thickness. These challenges highlighted the necessity for a simpler and more robust masking solution, directly motivating the final method adopted in this thesis. Ultimately, the most effective solution was also the simplest: a stencil. The process will be described in further detail in Section 2.2.2.

To determine the necessary segment length for the segmented yarn system, a representative braid sample was fabricated using the materials and braiding process described later in Section 2.3.2. Upon disassembly and careful measurement, the junction-to-junction spacing was found to be approximately 2.6 mm, thereby establishing the required segment length. Achieving precise segmentation at this scale within an already fabricated braid presents considerable practical challenges, especially considering that the tubular structure obscures visibility and accessibility to the yarn segments facing the internal axis where the SMA wire resides. This limitation further validates the decision, discussed previously, to perform yarn segmentation and junction placement before integration into the braided textile structure.

Approaches to electroplating

This work builds on the electroplating method developed by Hardianto et al. [94], who plated carbon fiber (CF) with nickel to create a CF-NiCF composite. Their process, like many lab-scale fiber electroplating techniques, was batch-based. While effective for small quantities, batch methods involve frequent manual

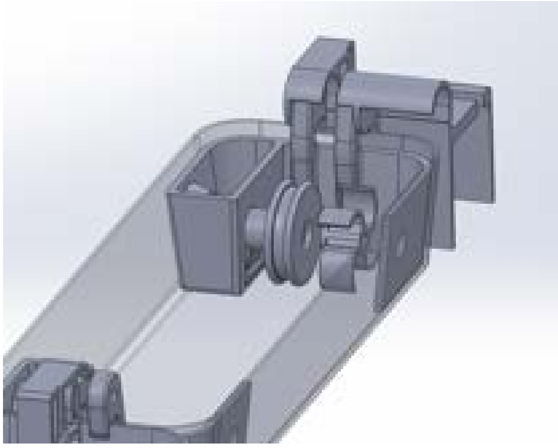

(a) CAD render of 3D printed components

(b) Cathode in use

Figure 2.4: Electrical contact for yarn nickel electroplating– Cathode assembly in nickeling bath

intervention, limited throughput, and reduced consistency across samples. These characteristics make them less suitable for producing longer yarns with uniform properties. To address this, a continuous electroplating approach was developed in this study with the intention of enabling longer yarns to be processed with minimal interruption, such that the yield becomes directly dependent on the duration of operation. Continuous methods also offer a more consistent and potentially scalable route for fiber functionalization, but they are less commonly implemented at the lab scale due to the added complexity in setup, maintaining electrical contact, and other conditions during operation. The setup thus must be designed to overcome these challenges while remaining compact and accessible for laboratory use.

Careful attention was given to the design of both the **anode** and **cathode** in order to avoid introducing unintended metal surfaces into the electrolyte during electroplating. It is essential that only the designated electrodes be exposed to the electrolyte while the plating circuit is closed and active. The presence of additional submerged conductive materials could disrupt the plating process, introduce unwanted side reactions, and degrade electrolyte performance. To mitigate this risk, all mechanical components in contact with the electrolyte were fabricated from plastic, including the 3D-printed rollers used to guide the yarn through the bath. Because fully plastic rotary bearings were not available, low-friction plastic bushing interfaces were used instead. Additionally, the cathode connection to the CF yarn was deliberately positioned outside the plating bath to further ensure that no unintended conductive paths were submerged. Electrical contact was established via a leaf spring pressing the yarn against a stationary copper plate, which was directly connected to the cathode lead of the power supply. In this arrangement, the electrical circuit was completed through the copper plate, ensuring a reliable connection to the yarn while maintaining full isolation of the electrical contact from the electrolyte solution. The bath system was designed in SOLIDWORKS and is shown in Figure 2.4.

As the yarn is continuously guided through the nickel electrolyte bath, each segment of the yarn is electroplated for the duration of its time submerged in the bath. This dwell time serves as a critical process parameter that directly influences the thickness and quality of the plated nickel layer. Since the yarn follows a consistent path through the bath, with uniform travel speed and immersion depth, this setup provides good repeatability and consistency in plating across the entire length of the processed yarn.

Approaches to yarn feeding and winding

The CF yarn was originally supplied on a large tubular yarn bobbin. To feed the yarn into the process, a simple yarn feeding mechanism adapted from a standard sewing machine was used; this system includes a freely rotating plastic spool holder designed for smooth thread unwinding. For the final winding stage, a standard sewing machine bobbin was selected due to its availability, affordability, and ease of integration into downstream processing equipment (the braiding machine). The winding system includes a 3D-printed plastic adapter to securely interface with the sewing machine bobbin.

The **winding mechanism** is responsible for continuously pulling the fibre through the entire electroplating process and was designed with hardware and software features that prioritize adaptability and precision in fibre electroplating applications. The hardware setup consists of the following components:

(a) CAD render of template

(b) Template in use

Figure 2.5: Masking template with segment length of 2.6mm

- Controller: Arduino Uno
- Motor: Micro Motors Geared DC Motor E192.12.18
- Motor Controller: Velleman Motor and Power shield KA03
- Screen: Velleman 0.96” OLED Display VMA438

The system’s human-machine interface (HMI) allows the user to control the motor-driven winding mechanism through an integrated organic light-emitting diode (OLED) display. This display provides a continuous readout of the motor’s rotational speed (RPM) along with a calculated estimate of the duration of time that the fibre would be submerged within the electroplating bath. The calculation accounts for the system’s gear ratio (which is determined by easily interchangeable gears within the setup) and the diameter of the winding bobbin, both of which directly influence winding speed and, consequently, the effective plating duration. The HMI is designed to give the user feedback by displaying the current motor RPM, previewing the change in RPM before confirmation, and providing the corresponding updated estimate for deposition time after the user confirms the new speed. This feedback allows the user to make informed adjustments to optimise plating consistency and process repeatability.

2.2.2 Proposed procedure for producing segmented Ni-NiCF yarn

Building upon the critical evaluation and exploratory development detailed in the preceding sections, this thesis proposes a continuous and scalable workflow for producing segmented Ni-NiCF yarn. This proposed method emphasizes simplicity, repeatability, and ease of implementation in a laboratory setting, while ensuring suitability for future scaling to industrial manufacturing environments.

Masking

The masking method ultimately implemented in this thesis involves a flat template/stencil, shown in Figure 2.5, that was designed in SOLIDWORKS to securely position and clamp the yarn between two precisely aligned halves. When the yarn is clamped, the template provides open slots on both sides that correspond to the desired segment length. These openings allow manual application of masking fluid using a fine-tipped brush. The masking fluid used is a 1:1 mixture of UHU brand water-based correction fluid and a generic paint varnish, selected for its excellent adhesion, flexibility, and electrical isolation performance. After the masking fluid is applied and allowed to set, the yarn is released by separating the template halves, repositioned, and then re-clamped to mask the next segment along its length. While this method is relatively slow and currently limited to masking lengths of approximately 10 cm at a time, it produces the most consistent and high-quality masks. Additionally, the yarn remains uncut during this process, enabling the masking operation to be extended as needed to support the subsequent continuous nickel plating process. Although this approach is not yet fully optimized for high-throughput production, it is sufficient for the scope of this thesis and supports further development of the segmented yarn system.

Nickeling

The final stage of the functionalization process involves selectively depositing a thin, conductive nickel layer onto the exposed segments of the masked CF yarn. This is achieved through an electroplating process, in which the yarn acts as the cathode within an electrolytic bath containing a nickel salt solution. The nickel electrolyte solution used in this thesis was from the brand Tifoo, MARAWE GmbH & Co. KG. When an electric current is applied, nickel ions are reduced and deposited onto the exposed conductive regions of the yarn.

The electroplating setup employed a thin sheet of pure nickel as the anode, positioned at the bottom of the plating bath and held in place with a pure nickel rod to ensure stable electrical contact. The CF yarn served as the cathode and was continuously submerged in the electrolyte solution as it was drawn through a pair of 3D-printed rollers. In this system, each segment of the yarn remains submerged – and thus actively electroplated – for 8 minutes as it passes through the bath. The most critical parameter for achieving uniform nickel deposition is the electroplating current, which was maintained at approximately 0.3 A using an external, manually controlled power supply. Steady current facilitates consistent nickel deposition across the exposed segments of the CF. During the plating process, the system operated at a voltage of approximately 3.0-3.5 V, as measured across the electrodes.

Following electroplating, the yarn passes through a secondary **wash bath** to remove any residual nickel salts from its surface. The washed fibre is then exposed to air to dry for approximately five minutes before being wound. This in-line washing and drying step is important both for safety (nickel salts are toxic) and for process efficiency, as it eliminates the need for a separate washing and drying stage.

Figure 2.6 illustrates the setup and key stages of the process developed in this thesis.

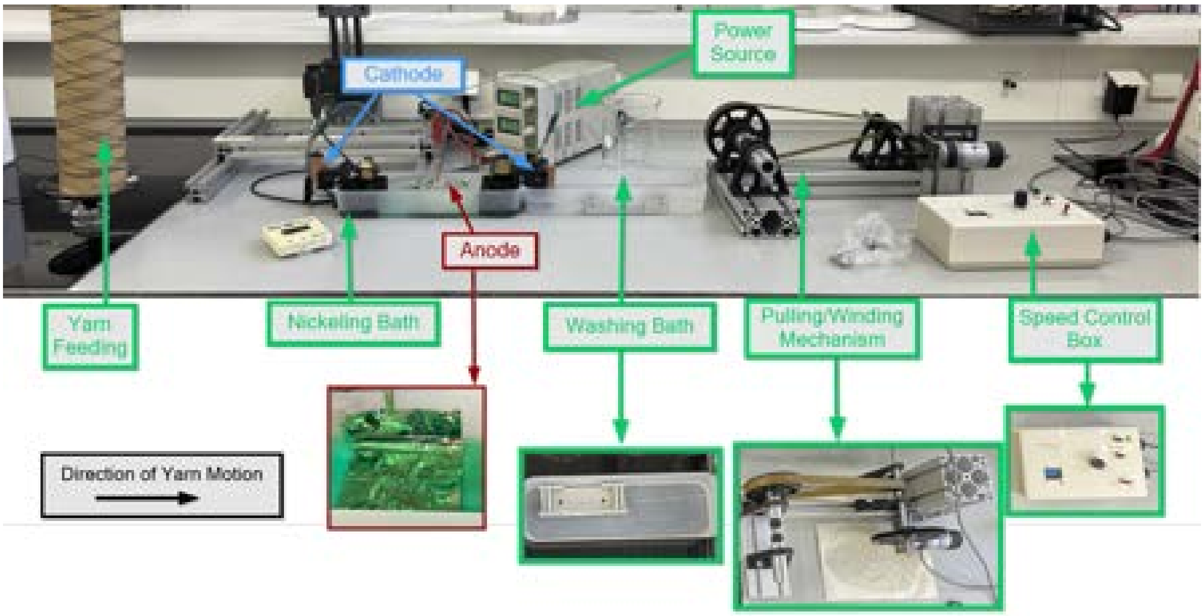

Figure 2.6: Image of continuous yarn nickeling process

The following procedure was used to set up and operate the electroplating machine for continuous nickel deposition on CF yarn:

1. Before setup, join approximately 0.5 m of silver-plated conductive yarn to the end of the functional CF yarn using a simple knot. Also, tie approximately 10cm of yarn to the sewing machine bobbin and secure the bobbin in the yarn winding mechanism.

2. Set up the machine components: place the yarn spool on the feeding mechanism, position the two tubs (nickeling and washing), and align the bobbin in the winding mechanism with the unspooling path of the yarn.

3. Connect the power supply leads to the anode and to both cathode assemblies.

Figure 2.7: Detail image of segmented and electroplated CF-NiCF yarn.

4. Power on the speed control box. Start the motor and adjust the speed control knob until the display shows a traversal time of 480 seconds for an 18 cm length. Once the correct speed is set, pause the motor.
5. Thread the yarn through the machine path: feed it through the cathode leaf springs, under the nickeling bath rollers, out of the first bath through the cathode leaf springs again, and under the rollers of the washing bath. Tie the two ends of the conductive yarn together; there should still be some slack at this stage.
6. Position the junction between the CF yarn and the conductive yarn under the first roller of the nickeling bath. Remove remaining slack by briefly starting the winding mechanism, allowing the yarn to become taut, and then pausing it again.
7. Fill the tubs: carefully fill the nickeling tub with nickel electrolyte until the yarn is fully submerged (avoid overfilling). Fill the washing tub with water until the rollers are submerged.
8. Switch on the power supply and quickly adjust the output until a current of approximately 0.3 A is flowing through the circuit. Start the winding mechanism at around the same time.
9. Allow the system to run until the desired length of yarn has been electroplated.
10. To finish the process as the spool nears its end, tie an additional piece of conductive yarn to the trailing end of the functional CF yarn to maintain electrical contact with the cathodes. Once the CF yarn has fully passed the water line in the washing bath, cut off any remaining slack, and allow the winding to complete before stopping the machine and removing the bobbin.

An image of the final electroplated yarn is shown in Figure 2.7. This section describes the electroplating parameters and experimental procedure used to produce the electroplated yarns for this thesis. It is important to note that the electroplating setup was intentionally designed to be freely adaptable, allowing it to be easily used for plating a wide variety of other conductive fibres without requiring further modification.

2.3 Braid structure

TexMind software is a braiding design tool that supported the early development of the braided device architecture presented in this thesis. While TexMind provided the necessary braid design and machine configuration parameters, the actual production of the braid required building a custom braiding machine from scratch – an effort that resulted in a lightweight machine that was almost entirely 3D-printed. With this machine and the finalized design, a TE braided device was fabricated using the functionalized yarn described in the previous section.

2.3.1 Braid design - Texmind

In this thesis, TexMind Braider [3] is used primarily to determine evenly spaced points along the braid surface that alternate between the outer and inner surfaces, as these points define the placement of the thermoelectric (TE) junctions. The software models the braid geometry based on key parameters such as yarn diameter, floating length, and number of yarns per group. Coordinating these parameters is crucial for achieving a compatible and manufacturable braid design, and TexMind provides a fast and effective way to check this during the design process. Additionally, TexMind has been instrumental in designing the computer-controlled braiding machine configuration. The software allows users to virtually follow the path of selected yarns through the braiding loop, providing an important visualization tool that accelerates early-stage development. This capability also ensures the correct positioning of carriers and yarns during machine setup.

Braiding design considerations

Achieving the desired braiding characteristics requires a comprehensive understanding of the underlying machine mechanisms and braiding principles, as outlined in Section 1.2.4. Several braid structures were iteratively prototyped virtually to estimate the achievable junction distance and density. While these estimates provide useful guidance, they are not used as final design values. As discussed in Section 2.2.1, measurements from a trial braid produced on the actual braiding equipment were ultimately used as the decisive reference for refining upstream design decisions, particularly regarding key parameters like the junction spacing of the functionalized yarn.

One key design decision was setting the number of floats per yarn to 3. This choice increases the spacing between junctions, resulting in a slightly lower junction density on the braid. With 12 yarns in total, and each yarn spending 3 floats on the outer surface and 3 on the inner surface per machine cycle, each yarn completes a predictable number of "surface crossover" transitions (two per cycle). This ensures that each full cycle of the machine results in a clean junction pattern: two n-p junctions on the inner surface and two p-n junctions on the outer surface per functional yarn. In contrast, using a float length of 2 would produce a braid with a smaller junction distance (only the thickness of two yarns), which leads to a high degree of manufacturing difficulty in the early stages of development. Selecting a float length of 3 increases the likelihood of achieving successful junction alignment along the braid, particularly given that no alternative braid alignment strategy was developed within the scope of this thesis.

Looking ahead, if junction alignment can be effectively addressed, the ideal braid configuration would employ a float length of two. This arrangement ensures that textile yarns can consistently provide electrical insulation between all functional yarns across the braid. Additionally, by assigning functional yarns to one-quarter of the total carriers, the braid would achieve the maximum possible junction density without necessitating changes to other braiding parameters, and this strategy can be generalized to circular braids of any size. TexMind's braiding machine configuration tools will assist in determining the appropriate starting carrier positions to implement this adjustment accurately.

Proposed braid design

The final braid design was selected to have a float length of 3 with yarns grouped in a single group. TexMind's computer-controlled braiding machine configuration software determined that a machine with four horn gears, each equipped with six carrier slots, would be needed to achieve the desired braid pattern, as illustrated in Figure 1.3. Although several braiding machines are available at ITM, their configurations do not match the aforementioned setup. Specifically, it is not possible to produce a float length of 3 using machines with six horn gears and four carrier slots per gear, as the arrangement of horn gears fundamentally limits the achievable float patterns. As a result, there was a clear need to develop a custom braiding machine to enable this design, as the desired horn gear configuration could not be realized with the existing equipment at the facility.

2.3.2 Braiding machine - CAD design and 3D printing

This section describes the design and construction of the custom braiding machine developed for this thesis. Based on the braiding configuration described previously, the machine was designed with four equally sized horn gears arranged in a configuration of two clockwise (CW) and two counterclockwise (CCW) gears, an arrangement achieved through a looped gear train. Each horn gear includes six carrier slots, in accordance with the requirements for the selected braid structure. Figure 2.8 presents both a CAD rendering of the machine and a photograph of the assembled system in operation.

The design of the braiding machine was guided by the design principles outlined by Y. Kyosev in "Braiding Technology for Textiles" [62]. In addition, certain design elements were inspired by lightweight, open-source braiding machines, which provided valuable insights into practical, 3D-printed construction approaches that aligned with the fabrication methods employed in this work [95, 96]. The CAD development for the machine was carried out using SOLIDWORKS. Many components were designed from scratch, while others were adapted from existing off-the-shelf mechanical component models (e.g., those available from suppliers such as McMaster-Carr), which served as a starting point for efficient and accurate design.

(a) CAD render of braiding machine (b) Braid machine in use

Figure 2.8: Braiding machine used for sample fabrication

The machine is powered by a manual hand-crank mechanism, which provides fine control that is especially important during the initial troubleshooting and calibration stages. The system employs a 1:3 gear ratio between the horn gears and the crank, such that one full rotation of the crank corresponds to a single yarn transfer step between the horn gears.

The design objective for this braiding machine was to achieve full functional operation while minimizing the volume of printed material required. As a result, several features commonly found on industrial braiding machines were intentionally omitted in order to prioritize simplicity and flexibility during early-stage development. For example, instead of incorporating an integrated take-up winding mechanism or an automated braid tensioning system, this machine relies on manual pulling and tension adjustment, which allows greater control and flexibility during prototyping. Similarly, no dedicated core feed mechanism was implemented; instead, the core filament is simply guided through a hole in the centre of the track and drawn along with the braid during operation.

Yarn Carriers

A CAD rendering and a photograph of the 3D-printed yarn carrier are shown in Figure 2.9. The yarn carriers are propelled around the track through mechanical engagement with slots in each horn gear. As the carriers traverse the track, they are transferred between adjacent horn gears at track intersections, enabling the formation of loops in the continuous braiding process. The base of each carrier features a long, convex lens-like profile that allows it to smoothly follow the 3D-printed track guide.

Proper yarn tensioning is crucial, as the yarn path length varies dynamically while the carriers move around the track due to them approaching (shorter) and receding away (longer) from the central axis. To manage this, each carrier incorporates an integrated tensioning mechanism: a single-print yarn bobbin base with a hinge designed to hold an M4 nut. The nut functions both as a yarn guide and as a counterweight, mounted at the end of a long hinged arm. This pivoting mechanism allows the arm to adjust dynamically, maintaining consistent yarn tension throughout the braiding cycle.

2.4 Device fabrication

This section describes the complete fabrication process of the braided Peltier device, detailing the materials used and the step-by-step procedure for constructing the final textile-integrated thermoelectric structure.

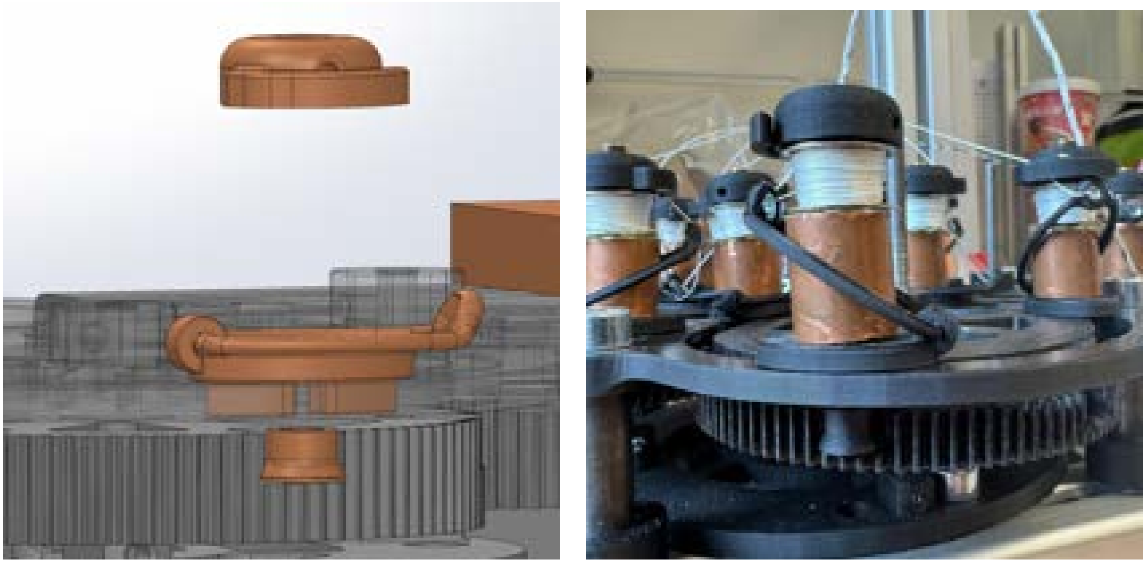

(a) CAD render of yarn carrier (b) Yarn carrier in use

Figure 2.9: Yarn carrier design used in braiding machine

2.4.1 Materials

Further details regarding the materials used in the braid composition are provided in Table 2.4. It should be noted that the core filament is a compound structure: it consists of the SMA wire wrapped in a TPU sheath. The TPU sheath was sourced by deconstructing a commercial TPU-coated conductive yarn product from the manufacturer Shieldex. The sheath was then carefully slipped over the SMA wire to provide electrical insulation within the braided structure. A photo of this arrangement is shown in Figure 2.10.

Table 2.4: Fibre materials used in braid: legend and specifications

Material	Manufacturer and Make
Nylon 66 Filament, 312 dtex, twisted	Barnet Europe
Segmented CF - NiCF	Toho Tenax Co., Ltd.
TPU tube	Shieldex (Deconstructed)
NiTi Wire (Flexinol), 0.012”	Dynalloy Inc

Figure 2.10: Detail image of NiTi Wire (Flexinol) with TPU sheath

2.4.2 Fabrication procedure

The following steps were completed to fabricate the braided device:

1. **Prepare the yarn carriers:** Wind 11 sewing machine bobbins with pre-twisted Nylon 66 yarn and insert them into the yarn carriers on the braiding machine. Prepare a twelfth bobbin using the functionalized yarn, as described in Section 2.2.1, and insert it into one of the carriers.

2. **Load the core into the machine:** Pass the TPU-wrapped SMA wire through the center of the braiding machine to act as the core filament.
3. **Start the braiding process:** Gather the yarn ends from all carriers and pin them together at the starting point. Begin manually rotating the hand crank to initiate braiding, ensuring a uniform and stable braid structure is established.
4. **Insert top crimp:** Once a consistent braid structure is achieved, slide a 4 mm diameter crimp onto the braided section. Crimp the top crimp at the point where the desired braid length should start.
5. **Continue braiding to target length:** Continue rotating the hand crank to extend the braid to at least 10 cm in length.
6. **Insert bottom crimp:** At a distance of 7 cm from the bottom edge of the first crimp, align and crimp the second 4 mm diameter crimp, such that the section of braid between the two crimps measures exactly 7 cm.
7. **Secure and cut the braid:** To prevent braid unraveling, use a clip to secure the section of braid below the second crimp. Carefully cut the braid with wire cutters, leaving approximately 20 mm of extra SMA wire protruding past the second crimp to allow for easy handling and later electrical connection.

2.5 Description of the device

The device developed in this thesis is a braided thermoelectric (TE) sheath surrounding a thermoplastic polyurethane (TPU)-coated nickel-titanium (NiTi) shape memory alloy (SMA) actuator wire. Its TE functionality is achieved by incorporating a single functionalized yarn into the braid. This yarn is fabricated with a segmented structure, alternating between segments of carbon fibre (CF) and nickel-plated carbon fibre (NiCF), forming a series of thermocouple junctions. The braid pattern positions these junctions alternately on the inner and outer surfaces of the sheath, enabling the device to operate as a heat pump via the Peltier effect. A photo of the completed device is shown in Figure 2.11.

Figure 2.11: Detail image of fabricated thermoelectric braid

3

Testing and characterization

The primary objective of the testing and characterization presented in this chapter is to evaluate the influence of the textile-integrated sheath on the actuation and recovery behavior of the SMA wire. Specifically, the tests aim to determine whether the TE effects provided by the sheath can be observed through changes in the mechanical tension, electrical signals, and thermal response of the system. The goal of the device is to improve the rate at which the SMA wire returns to its original state after heating. By systematically comparing different combinations of heating and cooling configurations, this chapter seeks to characterize how the sheath contributes to the overall performance of the device and to assess its potential as an active control mechanism in SMA-based actuators.

3.1 Setup

This section describes the experimental setup used to test the device prototypes developed in this thesis. The overall setup, shown in Figure 3.1, was designed to enable precise control of heating and cooling inputs, accurate measurement of mechanical and electrical responses, and synchronized collection of temperature and force data. For clarity, the key subsystems “SMA mounting”, “temperature measurement”, and “control and data collection” are discussed in the following subsections.

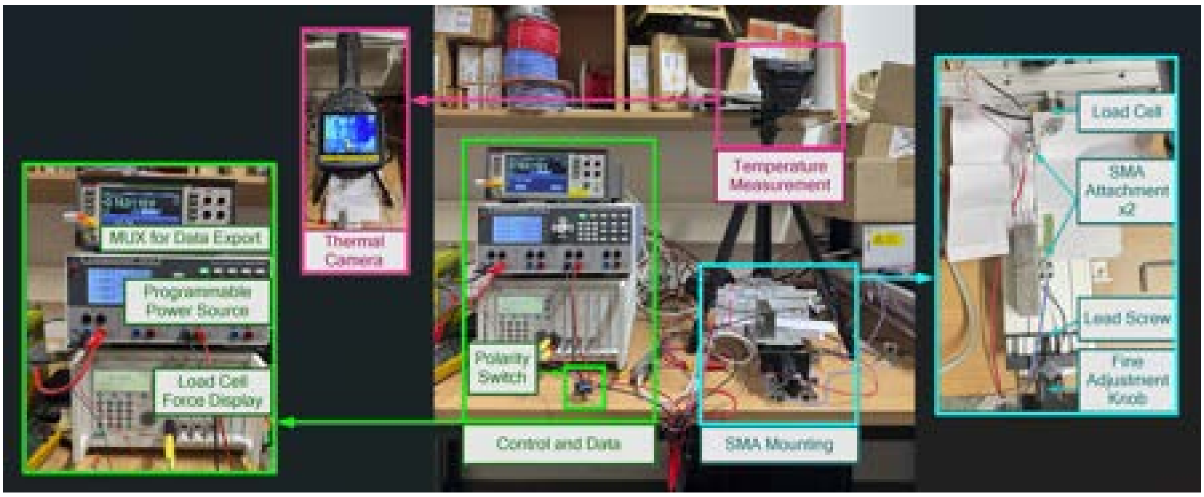

Figure 3.1: Experimental setup for device testing

SMA mounting

The SMA mounting assembly serves to secure the device samples during testing while providing stable mechanical attachments and electrical interfaces in order to monitor the voltage applied to the SMA wire core and the functional conductive yarn in the outer sheath.

Mechanical attachments at either end of the sample are made to bare (non-TPU-coated) sections of the SMA wire. The wire is clamped between the surface of a steel block and the head of a screw to provide a firm mechanical connection. One end of the sample is connected to the load cell, which measures the tension force generated during actuation. The opposite end is connected to a lead screw mechanism equipped with a fine adjustment knob. This allows precise control of the pretension applied to the sample during setup, ensuring consistent initial conditions across tests.

Electrical connections to the SMA wire and to the conductive sheath yarn are made at points interior to the mechanical attachment locations. This design minimizes the influence of any conductive elements present in the aluminum frame of the mounting assembly and prevents unintended electrical pathways through the mechanical fixtures.

Temperature measurement

Temperature measurements were performed using a single device: a FLIR E95 Pro thermal camera. The camera was mounted on a tripod and positioned to provide a full view of the braided sample, surrounding contact points, and electrical attachments. The center of the camera's viewfinder was aimed at the middle of the braid to monitor temperature at this key location. To improve the quality of the thermal images, a sheet of paper was placed beneath the sample along the surface of the metallic test frame. This reduced unwanted reflections caused by the infrared reflectivity of the metal and provided a more consistent thermal background for the measurements.

Video recordings of each test were captured and later exported for analysis. Using an open online *.csq* file viewing service, it was possible to extract temperature data from specific points in the recorded video as needed.

Control and data collection

The power supply used in this study allows for programmable control of both the inner SMA core and the outer functional yarn of the device. Independent voltage programs can be created for each component, enabling precise control of timing sequences for heating and cooling cycles as required for the different test configurations. A switch was connected to the power supply leads to allow the polarity applied to the outer functional yarn to be easily reversed during testing.

During testing, the load cell output is displayed in real time to provide immediate feedback to the operator. In addition to this live display, the load cell signal is simultaneously recorded using a data acquisition (DAQ) system from Keithley Instruments. This ensures that all load cell measurements are captured at high resolution for post-processing and analysis. The DAQ system also records voltage signals from the SMA core and the functional yarn sheath. All signals are synchronized and logged to CSV files for later processing in MATLAB, where tension profiles and activation timings are analyzed. This setup allows for flexible test design and high-quality data collection across all experimental configurations. The model and manufacturer of the specific devices used in this subsystem are as follows:

- Programmable power source with manual polarity switch: HMP4040 from Rohde & Schwarz
- Data acquisition system: DAQ6510 from Keithley Instruments
- Load cell data acquisition system (for static readings): MGCplus from Hottinger Baldwin Messtechnik
- Load cell: U9C from Hottinger Baldwin Messtechnik, up to 50N

3.2 Methodology

To evaluate the effect of textile-integrated Peltier cooling on the recovery dynamics of the shape memory alloy (SMA) actuator, several key experimental parameters were defined. These included the driving currents and activation profiles for both the SMA wire and the functional yarn as well as the overall test configurations to be compared. The goal was to maximize sensitivity to potential improvements in SMA recovery while minimizing confounding factors such as excessive Joule heating.

Based on this framework, four distinct test configurations were designed, each varying the heating and cooling mechanisms applied to the SMA wire and surrounding sheath. Each configuration has a specially designed driving current profile. These profiles control both the timing and polarity of the voltage applied to the yarn, and were tailored to the activation behaviour of the SMA wire or to implement independent cooling cycles. The driving profiles were implemented using programmable voltage outputs from the power supply, with separate channels for the SMA core and the functional yarn sheath. This allowed precise synchronization of heating and cooling phases across all tests. The configurations are summarized as follows:

Control Configurations

1. **Control** – Resistive heating with braided sheath using conductive yarns – In this baseline test, voltage was applied to the SMA wire for 5 seconds every half a minute to induce contraction, and the surrounding sheath was composed of standard conductive yarns which provided no additional functionality, i.e., no TE yarn was used in this configuration. A photo of the prepared sample for this configuration is shown in Figure 3.2.

2. **Passive Peltier sheath** – Resistive heating and Peltier-functional yarn sheath – Similar to the control, voltage was applied to the SMA wire for 5 seconds every half a minute. In this case, the sheath was constructed from functional yarns theoretically capable of the Peltier effect, but no active cooling was applied; the test aimed to observe any passive or incidental effects on the sheath voltage during SMA heating.

3. **Peltier-only cycling** – Peltier Heat, Peltier cooling – In this configuration, no direct resistive heating was applied to the SMA wire. Instead, the functional yarn sheath was actively driven using a polarity-reversing voltage to create cycles of heating and cooling through the Peltier effect.

4. **Peltier cooling** – Resistive heating with Peltier cooling – The SMA wire was resistively heated for 5 seconds at a lower current of 0.5 A. The Peltier-functional sheath is actively driven to accelerate the wire's recovery phase at a pattern of 15 seconds on, 15 seconds off. This configuration directly tests whether active Peltier cooling improves recovery compared to the control.

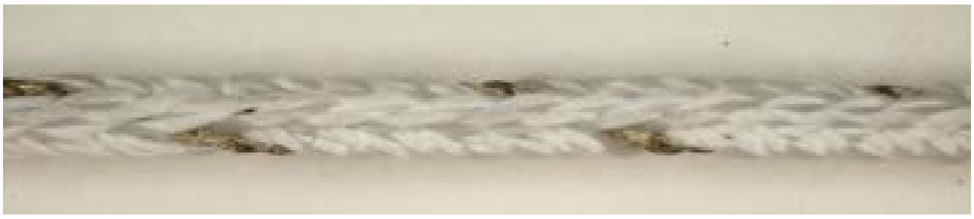

Figure 3.2: Detail image of control braided sample with silver-plated yarn

Functional yarn driving current

As described in Equation 1.1, the energy generated by Joule heating increases quadratically with the applied current. Previous work has established that one of the primary limitations of the functional yarn is its sensitivity to excessive Joule heating, which counteracts its thermoelectric performance. Therefore, it is critical to minimize the driving current used during operation to prevent unwanted heat generation.

To identify a suitable operating range, several currents between 0.1 A and 0.3 A were tested. As expected, higher currents produced correspondingly greater heat in the yarn regardless of polarity through the TE yarn. However, for 0.1 A there were no significant effects one way or another. Based on these tests, a driving current of 0.2 A was selected for use in Peltier cooling configurations in order to balance the desired cooling effect against the risk of excessive self-heating in the yarn.

SMA driving current

This section outlines the process used to determine an appropriate driving current for the SMA wire. In all tests, the SMA wire was pretensioned to 2 N prior to activation. Pretensioning ensures a consistent mechanical response and improves the repeatability of the actuation by maintaining the wire within its optimal working range.

To identify a suitable driving current, a baseline activation duration of 5 seconds was established, and a series of currents were tested. The goal was to select a current that would produce a peak tension near the upper quartile of the load cell's sensitivity range without exceeding its maximum capacity for all the test configurations. The load cell used in this study had a full-scale range of 50 N.

Based on these tests, a driving current of 1.6 A applied for 5 seconds was selected. This configuration consistently produced peak tensions reaching approximately 70% of the load cell range in the baseline control configuration, providing sufficient dynamic range to observe both increases and decreases in tension under different experimental conditions.

For the Peltier cooling configuration, the driving current for the SMA wire needed to produce a stable steady-state temperature and tension. Several currents were applied to the control configuration, and 0.5 A was selected to best match this requirement.

4

Results and discussion

This chapter presents the results of four experimental configurations designed to evaluate the thermal and mechanical performance of the textile-integrated Peltier cooling system. Each configuration is presented with temperature data, thermal imaging, and key performance observations. The section concludes with a critical discussion of the findings.

4.1 Review of configurations

This section presents key insights from each configuration test, highlighting trends and performance differences. A more comprehensive overview of all results is provided in Appendix B.

Control vs. passive Peltier sheath

The CF functional fibres for both the control and the passive peltier sheath configuration were driven using a repeating cycle of alternating voltage polarity: a 5-second heating phase with a positive voltage, followed by a 25-second rest period, then a 5-second cooling phase with reversed polarity, followed by another 25-second rest period. This cycle was repeated throughout the test for several cycles. The relative force change resulting from SMA activation for each cycle is shown in Figure 4.1, where all cycles are overlaid. Blue lines represent the configuration with the TE functional yarn sheath, while green lines represent the control configuration, which used only conductive yarns.

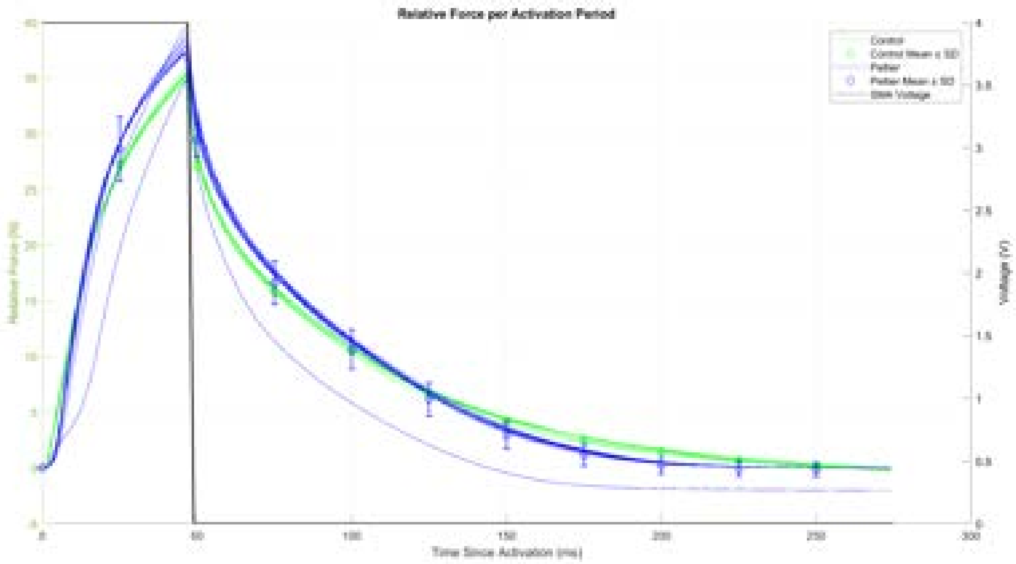

Figure 4.1: Comparison of force response for cyclical actuation and cooling for the control and passive Peltier configurations

The results show that the Peltier-integrated sheath exhibits a faster rise time, reaching peak tension more quickly and achieving higher force output under the same current conditions. This may be partially attributed to the current-driven nature of the system, where slight differences in electrical resistance between the two configurations could lead to increased resistive heating in the Peltier sample. This interpretation is supported by the observation that the voltage across the Peltier-integrated sample was consistently higher than that of the control, indicating a higher power input. During the cooling phase, the force decreases with a steeper slope in the Peltier case, suggesting that the thermoelectric sheath contributes to more effective passive cooling. These findings suggest that, even in the absence of active thermoelectric control, the Peltier sheath may enhance both heating and cooling dynamics, thereby improving overall actuation performance.

To further quantify the thermal effects, the area under the curve (area under the curve (AUC)) for each cycle was calculated in MATLAB as a proxy for total heat energy, based on the assumption that force response is strongly correlated with heat flow. A two-sample t-test was conducted on the AUC values, as detailed in Appendix B. While the difference was not statistically significant, the mean AUC for the control configuration was slightly higher (96.5) than that of the Peltier sheath (95.6). This small but consistent trend suggests that the Peltier sheath may facilitate more efficient heat dissipation, potentially reducing thermal load while enhancing actuation performance.

Peltier heating and Peltier cooling

This configuration alternated between Peltier heating and cooling modes without activating the SMA wire, in order to isolate and observe the effects of Joule heating in the carbon fiber (CF) functional yarn. The polarity of the current (and thus the direction of the thermoelectric effect) was manually controlled, and as such, the switching did not follow a fixed time interval. Instead, time stamps from the thermal imagery were correlated with corresponding points in the electrical and force data to assess how the Peltier sheath influenced temperature distribution over time.

Load cell measurements confirmed that the thermal input from the Peltier sheath alone was insufficient to trigger actuation of the SMA wire. This indicates that the resistive and thermoelectric heating within the sheath, under the tested current levels, does not raise the temperature of the SMA to its activation threshold. It is important to note here that further increases in current in this system would be a fire hazard. As a result, the tensile response remains largely unaffected under safe operating conditions during this test condition.

Supporting thermal imagery from this test is shown in Figure 4.2. These images illustrate the thermal response over time as the functional yarn undergoes active heating. After approximately two seconds, the central region of the braided sheath reaches a temperature of around 34.4 °C, indicating the onset of thermal activation in the functionalized yarn. Notably, the area adjacent to the metallic crimp near the electrical connection on the positive lead heats more rapidly, attaining temperatures up to 54.8 °C at the same time frame.

This rapid temperature rise in the functionalized carbon fiber (CF) yarn confirms that Joule heating is active and localized primarily along the yarn pathway. The initial heat concentration near the crimps is attributed to their proximity to the electrical contacts and their higher thermal conductivity. As heating continues, the temperature distribution across the braided structure begins to equilibrate. By approximately seven seconds, thermal conduction into the surrounding Nylon 66 fibers becomes evident, with the sheath approaching thermal uniformity. At this stage, peak temperatures reach up to 60.4 °C.

Resistive heating with Peltier cooling

In Configuration 4, Peltier cooling was applied concurrently with Joule heating of the SMA wire. The functional yarn operated in active TE mode, with the current polarity configured to enable thermoelectric heat pumping. Simultaneously, a constant current of 0.2 A was supplied to the SMA wire to maintain a relatively steady-state mechanical tension.

Both the cooling and heating modes of the Peltier yarn were tested in this configuration. According to the device setup, positive voltages correspond to heating (where the SMA-facing side of the yarn functions as the heat sink) while negative voltages correspond to cooling (where the SMA-facing side absorbs heat). Figure 4.3 compares the resulting force profiles for both polarities. In the graph, red lines represent heating-mode periods, and blue lines represent cooling-mode periods. Visual inspection of the data suggests that the heating mode tends to produce a more rapid and greater increase in mechanical tension compared to the cooling mode. This trend is further supported by the time-resolved average profiles, also shown in the figure.

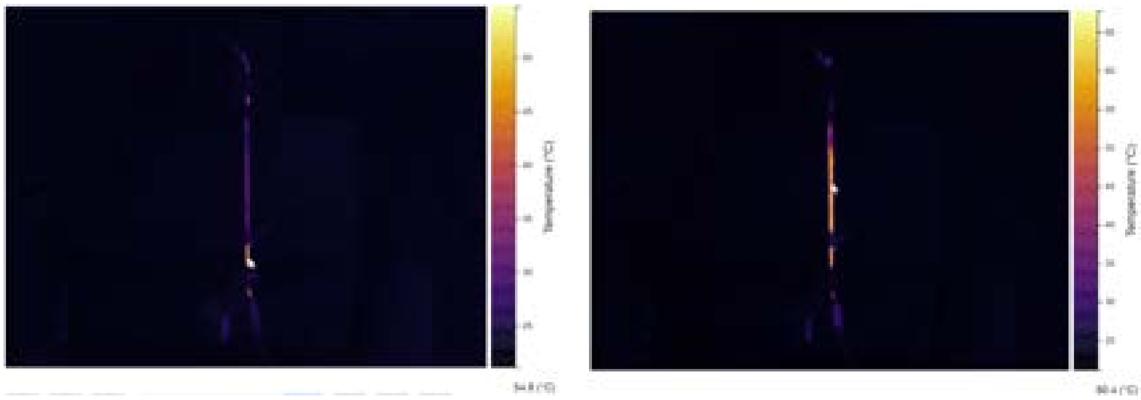

(a) Initial heating after 2 seconds (b) Peak temperature after 7 seconds

Figure 4.2: Thermal imagery showing temperature distribution during the start of the Peltier-only cycling configuration

To quantitatively assess whether this observed difference is statistically significant—a key consideration for validating the directional thermoelectric functionality—a two-sample t-test was conducted using the area under each relative force curve as a proxy for mechanical output. The AUC captures both the magnitude and duration of the force response, offering a robust scalar metric for comparison. As the Peltier effect is strongly dependent on the direction of electric current, the reversal of polarity should theoretically reverse the heat flow direction, thereby altering the thermal gradient across the SMA and impacting its contraction dynamics.

The t-test was performed in MATLAB, with the results detailed in Appendix B. Despite the apparent difference in average force trends between heating and cooling modes, the analysis showed no statistically significant difference in AUC between the two conditions. This suggests that while Peltier polarity clearly influences the thermomechanical behavior of the system, the active cooling effect may be insufficient to counteract the heat generated by resistive SMA activation.

4.2 Discussion

While the results show promising trends in actuation performance and thermal response, the broader takeaway is more sobering: with the current device configuration, Joule heating remains an unavoidable and dominant factor. Despite efforts to enhance thermal management and integrate thermoelectric functionality, the system is ultimately limited by its inability to effectively dissipate excess heat. It is likely that limitations in cooling efficiency, thermal contact, or a lag in heat extraction relative to the SMA's contraction kinetics reduce the net cooling impact. This section discusses the key design factors contributing to this limitation and outlines opportunities for improving heat management and system efficiency in future iterations.

4.2.1 Heat dissipation and mounting design

Thermal imaging revealed that the surrounding aluminum mounting frame experienced a noticeable increase in temperature during SMA activation. This suggests that a substantial portion of the generated heat is being conducted away from the SMA wire and into the frame, creating an unintended energy loss pathway. Such conduction not only reduces actuation efficiency but also interferes with the thermal gradients necessary for effective thermoelectric (TE) operation within the braid.

Additionally, the SMA wire was crimped into the system using a metallic connector. Based on the thermal imaging results shown in Figure 4.2, it appears to serve as an additional low-resistance pathway for heat transfer. The metal crimp likely accelerates local heating due to its high thermal conductivity, further complicating attempts to manage temperature distribution in the system. Together, the frame and crimp contribute to unwanted heat sinking that competes with the desired thermal behavior of the device.

To address these issues, future designs should prioritize the use of thermally and electrically insulating materials at mechanical interfaces. For instance, mounting the SMA wire using a high-temperature

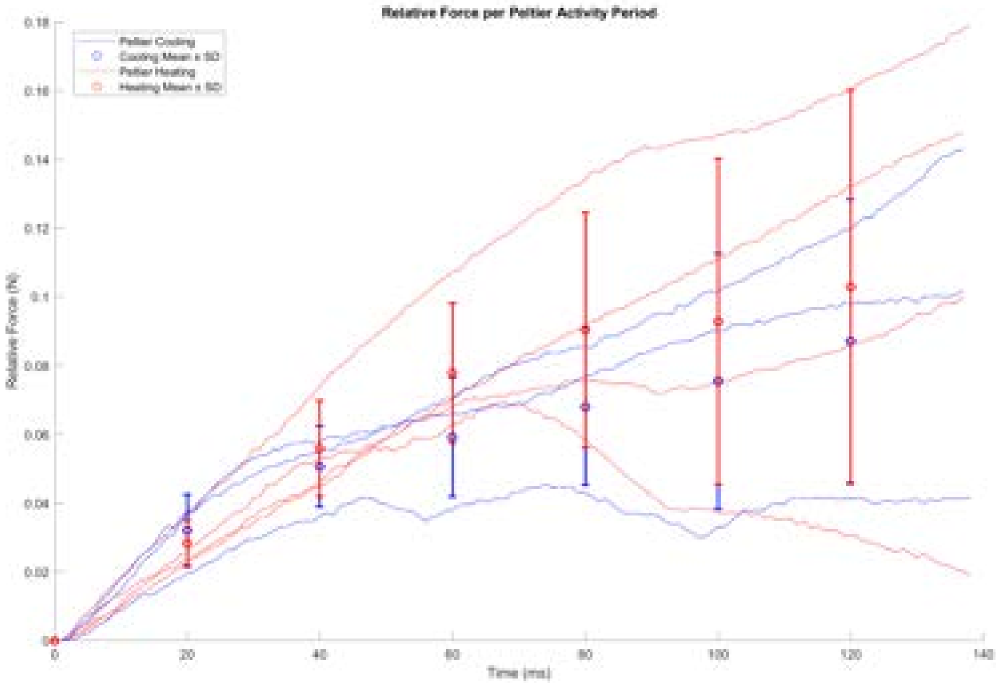

Figure 4.3: Comparison of force response during active Peltier heating (red) and cooling (blue) under constant resistive activation of the SMA wire

polymer would reduce thermal leakage into the rig and help preserve the localized heat required for actuation.

4.2.2 Limitations and opportunities in thermocouple material selection

As discussed in Section 2.1.3, the thermocouple materials used in this project were selected based on manufacturing feasibility rather than optimal TE performance. The final pairing of CF and NiCF exhibited a relatively low Seebeck coefficient of $8\,\mu V\,K^{-1}$ (Table 2.2), which significantly limits the efficiency of the Peltier effect in this design. For comparison, Hardianto et al. [94] reported a Seebeck coefficient of $19.22\,\mu V\,K^{-1}$ for the same material pairing, suggesting that refinements to the nickel plating process or CF substrate selection could improve performance.

Beyond improving the current CF-NiCF process, exploring entirely different thermocouple material pairings represents a promising direction. As summarized in Table 1.1, several materials found in literature exhibit Seebeck coefficients more than twenty times greater than those achieved in this study. In future iterations of the device, TE performance could be significantly enhanced by prioritizing these high-performance materials. Approaches from semiconductor doping and other advanced material design techniques may be especially valuable if the device efficiency becomes a primary design goal.

Finally, measurements in Table 2.2 suggest that metal-to-metal thermocouple junctions often exhibited higher Seebeck coefficients than yarn-based pairings in this work. As a result, incorporating metal-based thermocouples—either in combination with or as an alternative to yarn-based structures—could be a worthwhile avenue for improving the performance of textile-integrated TE systems.

4.2.3 Mechanical stability of thermoelectric junctions

Another observed limitation was the mechanical instability of the thermocouple junctions embedded in the braid. Under mechanical strain or repeated actuation, the junctions were found to shift, potentially changing their location relative to the braid and reducing device consistency and effectiveness. Future designs should address this issue by incorporating mechanical stabilization strategies. One concept is to embed the junctions into conductive beads, which can then be electrically connected in parallel to a common conductor. This would help maintain their location and function, even under strain, while allowing for distributed electrical contact across the sheath.

This page is intentionally left blank.

5

Conclusion and future steps

This thesis investigated the potential of textile-integrated Peltier cooling to enhance the performance of shape memory alloy (SMA) actuators, with a focus on improving the recovery dynamics of SMA wires through active thermal management. Beginning with a comprehensive literature review, this work established the foundational concepts of SMA behavior, thermoelectric effects, and current approaches to textile integration. This background informed key decisions in material selection, braid architecture, and testing methodology.

Subsequently, a fabrication system was designed and implemented to produce the functional yarns and braided structures required for this application. A systematic exploration of thermocouple materials was conducted, including the measurement of Seebeck coefficients and evaluation of mechanical and thermal compatibility with the braiding process. These efforts led to the development of a complete device fabrication workflow encompassing yarn production, braid design, and prototype assembly.

To assess the feasibility and impact of this approach, four controlled test configurations were developed to isolate the effects of various heating and cooling mechanisms on SMA actuation. These tests enabled a preliminary evaluation of how active Peltier cooling influences both the thermal and mechanical behavior of the system.

Future testing

While this work provides an initial demonstration of the concept, additional testing is required to more robustly characterize system performance. The current prototypes represent first-generation samples, and improvements in fabrication consistency, material integration, and assembly methods will enhance reliability and repeatability.

Future work should include: long-term durability testing under cyclic loading; exploration of variations in braid geometry and tension; evaluation of different thermoelectric materials and braid architectures; and expansion to larger sample sets for statistical analysis. Comparative benchmarking with prior literature can also yield insights into device optimization. For example, Churchill et al. conducted thermoelectric control studies on the same NiTi wire used in this project, offering a useful performance reference for future refinement of the cooling strategy and thermoelectric integration methods [97].

In addition, further mechanical characterization of the functional yarns is essential. The nickel plating process may alter key properties such as tensile strength, stiffness, or abrasion resistance, which could impact both braid performance and long-term durability. Quantifying these mechanical changes will help determine whether the plating introduces any trade-offs that must be addressed in future designs, especially for wearable or high-cycling applications.

Future system development

An important next step for advancing this technology is the development of a closed-loop control system to coordinate temperature regulation and actuation. Such a system would dynamically adjust cooling profiles in response to the actuator's thermal state, enabling more efficient and adaptive behavior. While this project initially included a Simulink model to explore system-level dynamics, it was ultimately excluded from the thesis scope due to the extensive calibration required. However, this modeling effort underscores the value of simulation as a tool for future optimization, and it remains a critical area for further development.

Final Remarks

This thesis has demonstrated the feasibility of incorporating active thermoelectric cooling into a textile-based SMA actuator system. Through a combination of systematic material investigation, novel device fabrication, and controlled performance testing, it lays a strong foundation for continued exploration and optimization.

Looking forward, the integration of thermoelectric cooling within smart textiles has the potential to unlock faster, more responsive, and more energy-efficient actuation for wearable and robotic applications. As wearable technologies continue to demand lightweight, silent, and compact actuation systems, the ability to thermally manage SMA performance via integrated textile structures represents a significant advancement — one that bridges material science, textile engineering, and functional design.

6 Societal Reflection

I would like to take a moment to reflect on the spirit behind this work and on the broader opportunities and challenges I have observed in the world of textiles. This project — developing a braided thermoelectric (TE) textile for active cooling in shape memory alloy (SMA) actuators — is not only technically novel, but also represents an attempt to expand the way we think about what textiles can be. More than once, as I was building the functionalized yarn into the braid, I realized that the potential didn't stop at creating a braid with a functional yarn — what I truly wanted was a prototyping platform for smart textiles as ubiquitous and accessible as the electronic breadboard. My goal was to design something that plays to the strengths of the textile form factor: not simply passive materials, but active, functional components integrated into complex engineered systems.

Just as Facebook cured loneliness on a cold college campus and all the problems of modern living became solvable with an app, a visionary in the 1980s sold chairs entirely molded from plastic, and ever since then, the solution to every product design engineer's problem is clips on a 1.8 mm-thick plastic substrate. However, I would argue that this ubiquity reflects not superior suitability, but the ease of access; perceptions of innovation are often shaped by what is readily available to prototype and produce. Textiles are perceived by other engineering disciplines as "niche" or even a passing "trend", as in the automotive interiors industry, where textiles have recently become popular again as it incites consumer perceptions of eco-friendliness. This characterization felt deeply wrong to me. After all, textiles were central to the industrial revolution itself... it is one of modern humanity's oldest technologies, yet despite its foundational role in our civilization, it doesn't appear accessible to product engineers. Therefore, since additive manufacturing has made prototyping with plastics feel simple and affordable, we develop more and more plastic products. Textile prototyping remains slow, costly, and limited to large manufacturers, which reinforces the perception that textiles are specialized and difficult to work with. In this thesis, I developed a lab-scale prototyping process for the fabrication of plated yarn and braiding textiles with the intention of easing access to prototyping platforms for rapid textile development.

Paul Fieguth's textbook on complex systems [98] has been a foundational influence on my thinking. He emphasizes the importance of recognizing patterns and transferable insights across domains, and I found his remarkably universal framework for systems analysis both elegant and deeply applicable to my own work. In today's world, problems are increasingly globalized and interrelated, so solutions must be as well. I often worry that opportunities in textiles are missed because fields such as electronics, robotics, and materials science continue to evolve in parallel, without considering textiles as a viable foundation for solving their challenges. Unlike the plastics industry, which has established clear conventions regarding the strengths and applications of its materials, textiles lack a similarly shared understanding across disciplines. In this thesis, I sought to address that gap: in the literature review, I intentionally added commentary on how novel technologies — even when their original authors had not envisioned textile applications — might be adapted to textile form factors. Interdisciplinary cooperation is not merely an opportunity; its absence is concerning. I often reflect on a paper from the medical field that described a curve estimation algorithm equivalent to the trapezoid rule — a basic concept from calculus — which the author insisted was novel in that context. Such gaps in cross-disciplinary awareness are troubling, and as fields grow ever more specialized, I live in fear that one day I will lose the commitment to recognizing valuable connections beyond our immediate domains.

In reflecting on this thesis, I also see a divide between academic and industrial approaches to problem-solving. Academic research often starts from first principles, while industry prioritizes user needs and manufacturability in a "product-first" mindset. The most extreme example of a product-first discipline is industrial design; these teams frequently lack technical background as detailed engineering considerations are viewed as potential constraints on user-centered creativity. In modern consumer products, industrial design and engineering teams work in parallel, each bringing distinct perspectives and ultimately meeting in the middle. Both perspectives are valuable, yet in academic institutions, these disciplines are disconnected with little structured collaboration. Early in this thesis, I had the opportunity to discuss this with Dr. Hung Le Xuan, who expressed his appreciation for a "backwards approach" — beginning with product requirements — and his observation at how uncommon this mindset remains in academic environments. The book Universal Methods of Design [99] reminds us that there are at least a hundred ways to approach any problem. Why not bring that same diversity of methods into technical research? In this thesis, I aimed to do so. The development of the braided TE textile involved rigorous engineering work, but was always informed by the practical goal of improving SMA actuator integration for real-world applications. Every design choice was made with usability and the needs of the end user in mind.

I also hope that this approach to engineering reflects a new-wave mindset towards sustainability. Many of the steps we take towards sustainable engineering today are not with the intention of making products better. Over time, this has eroded expectations of what a "good product" should be, and I fear that has a negative impact on our world. I believe the best approach to sustainability is to make the best possible product for each application and to use that best product more. Engineers should thus feel empowered to work across a wide scope of materials and design strategies. For example, a design engineer trained in injection molding (as I was) may see every design problem through that lens and arrive at injection-molded solutions by default – so their optimized product will progressively get thinner, more fragile, and harder to repair. But through this degree, I have come to see that many design challenges are ideally suited to textile form factors. If the best product for the job is a textile, then we should be making textile products that are actually the best for the job. Sustainability shouldn't just be about tiptoeing around the harm humanity does by our existence, it should also be about raising the standard of what we make and choosing better tools to meet that standard.

I remember being surprised during one of my master's courses when a vision of the future of the textile industry was described as something so distant we would "never see it in our lifetime." This struck me as deeply defeatist. Aren't we, as students in a graduate programme, precisely the ones meant to move it forward? Ultimately, textiles live in strange paradoxes like this all the time. They are one of humanity's oldest technologies, yet their production continues to grow every year. Perceptions of textiles remain limited, yet people don't live a single second of their lives separated from a textile product. The future of textiles depends on our ability to reimagine them as functional, structural, and active components within advanced systems. In developing the braided TE textile for SMA actuation, I hope this thesis offers a small example of how such reimagining can take place. My approach to this work has been shaped by two unlikely sources: a book on universal design methods and a book on complex systems. Together, they reflect a belief that innovation comes from systems thinking, interdisciplinary collaboration, and the courage to seek out unexpected sources of inspiration to solve impossible challenges. It is in that spirit that I hope this work contributes to the future of textiles.

Bibliography

[1] C. Lexcellent, *Some General Points about SMAs*, ch. 1, pp. 1–9. John Wiley & Sons, Ltd, 2013.

[2] D. Rowe, *CRC Handbook of Thermoelectrics*. CRC Press, 1995.

[3] TexMind UG, "TexMind Braiding Machine Configurator." `https://www.texmind.com/`, 2022. Rev 2022-02-09. Dresden, Germany.

[4] F. F. J. Luji, K. T. Teo, S. Tan, and H. Yoong, "Heating and cooling mechanisms for SMA actuator - a brief review," *Transactions on Science and Technology*, vol. 8, no. 3-3, pp. 425–431, 2021. UMS Colloquium on Fundamental Research and Applications 2020 (UMS Co-FA2020).

[5] Y. Lu, X. Fan, J. Luo, W. Liu, and L. Zhao, "Application of thermoelectric cooling on chip thermal management," *Kuei Suan Jen Hsueh Pao/Journal of the Chinese Ceramic Society*, vol. 53, pp. 849 – 861, apr 2025.

[6] M. Jancer, "Review: Embr wave." `https://www.wired.com/review/embr-wave/`, Feb 2020. Accessed: 2025-05-03.

[7] Y. Jing, M. Du, P. Zhang, Z. Liang, Y. Du, L. Yao, H. Chen, T. Zhang, and K. Zhang, "Advanced cooling textile technologies for personal thermoregulation," *Materials Today Physics*, vol. 41, 2024.

[8] U. Sajjad, K. Hamid, T. ur Rehman, M. Sultan, N. Abbas, H. M. Ali, M. Imran, M. Muneeshwaran, J.-Y. Chang, and C.-C. Wang, "Personal thermal management - a review on strategies, progress, and prospects," *International Communications in Heat and Mass Transfer*, vol. 130, 2022.

[9] D. T. Duy, V. N. Duy, N. T. Tan, V. M. Dien, and P. H. Binh, "A comprehensive review of advances in thermoelectric generators: Novel materials and enhanced applications for sustainable transportation," *International Journal of Thermofluids*, vol. 25, 2025.

[10] A. Bhattacharyya, D. C. Lagoudas, Y. Wang, and V. K. Kinra, "Thermoelectric cooling of shape memory alloy actuators: theoretical modeling and experiment," in *Proceedings of SPIE - The International Society for Optical Engineering*, vol. 2427, pp. 198 – 217, 1995.

[11] A. Bhattacharyya, D. Lagoudas, Y. Wang, and V. Kinra, "On the role of thermoelectric heat transfer in the design of sma actuators: Theoretical modeling and experiment," *Smart Materials and Structures*, vol. 4, no. 4, pp. 252 – 263, 1995.

[12] A. Bhattacharyya and D. Lagoudas, "Thermoelectric shape memory alloy actuators and the issue of thermomechanical coupling," in *Journal De Physique. IV : JP*, vol. 7 of *5*, pp. C5–673–C5–678, 1997.

[13] D. Lagoudas and A. Bhattacharyya, "Modeling of thin layer extensional thermoelectric sma actuators," *International Journal of Solids and Structures*, vol. 35, no. 3-4, pp. 331 – 362, 1998.

[14] M. M. Khan, D. C. Lagoudas, and O. K. Rediniotis, "Thermoelectric sma actuator: Preliminary prototype testing," in *Proceedings of SPIE - The International Society for Optical Engineering*, vol. 5054, pp. 147 – 155, 2003.

[15] O. J. Godard, M. Z. Lagoudas, and D. C. Lagoudas, "Design of space systems using shape memory alloys," in *Proceedings of SPIE - The International Society for Optical Engineering*, vol. 5056, pp. 545 – 558, 2003.

[16] G. S. Bushnell, D. Arbogast, and R. Ruggeri, "Shape control of a morphing structure (rotor blade) using a shape memory alloy actuator system," in *Proceedings of SPIE - The International Society for Optical Engineering*, vol. 6928, 2008.

[17] J. Abadie, N. Chaillet, C. Lexcellent, and A. Bourjault, "Thermoelectric control of shape memory alloy microactuators: A thermal model," in *Proceedings of SPIE - The International Society for Optical Engineering*, vol. 3667, pp. 326 – 336, 1999.

[18] J. Abadie, N. Chaillet, and C. Lexcellent, "An integrated shape memory alloy micro-actuator controlled by thermoelectric effect," *Sensors and Actuators, A: Physical*, vol. 99, no. 3, pp. 297 – 303, 2002.

[19] J. Abadie, N. Chaillet, and C. Lexcellent, "Bending model of an integrated sma micro-actuator," *Journal of Intelligent Material Systems and Structures*, vol. 15, no. 8, pp. 601 – 609, 2004.

[20] J. Abadie, N. Chaillet, and C. Lexcellent, "Modeling of a new sma microactuator for active endoscopy applications," in *IFAC Proceedings Volumes (IFAC-PapersOnline)*, vol. 12, 2006.

[21] J. Abadie, N. Chaillet, and C. Lexcellent, "Modeling of a new sma micro-actuator for active endoscopy applications," *Mechatronics*, vol. 19, no. 4, pp. 437 – 442, 2009.

[22] S. Jeong, G. Kim, S. Im, W. Jang, and K. Lee, "A study on control of shape memory alloy wire used in actuator of soft gripper," in *39th International Symposium on Robotics, ISR 2008*, pp. 672 – 675, 2008.

[23] A. Shelyakov, D. Rozhkov, N. Sitnikov, A. Menushenkov, A. Timofeev, and M. Berezin, "Micromechanical device based on amorphous-crystalline tinicu alloy," in *Materials Today: Proceedings*, vol. 4 3, pp. 4870 – 4874, 2017.

[24] Y. Luo, T. Takagi, S. Maruyama, and M. Yamada, "A shape memory alloy actuator using peltier modules and r-phase transition," *Journal of Intelligent Material Systems and Structures*, vol. 11, no. 7, pp. 503 – 511, 2000.

[25] T. Yambe, S. Amae, S. Maruyama, Y. Luo, H. Takagi, S.-S. Nanka, A. Tanaka, N. Kamiyama, R. Ohi, K. Tabayashi, H. Takeda, M. Yamada, and S.-I. Nitta, "Application of a shape memory alloy for internal artificial organs," *Journal of Artificial Organs*, vol. 4, no. 2, pp. 88 – 91, 2001.

[26] S. Maruyama, R. Ibuki, S. Sakai, M. Yamada, M. Sato, T. Yambe, T. Takagi, Y. Luo, and M. Behnia, "Development of a novel artificial heart muscle using thearmoelectric actuators," *International Journal of Heat and Technology*, vol. 19, no. 2, pp. 75 – 80, 2001.

[27] T. Yambe, Y. Shiraishi, M. Yoshizawa, A. Tanaka, K.-I. Abe, F. Sato, H. Matsuki, M. Esashi, Y. Haga, S. Maruyama, T. Takagi, Y. Luo, E. Okamoto, Y. Kubo, M. Osaka, S. Nanka, Y. Saijo, Y. Mibiki, T. Yamaguchi, M.-I. Shibata, and S. Nitta, "Artificial myocardium with an artificial baroreflex system using nano technology," *Biomedicine and Pharmacotherapy*, vol. 57, no. SUPPL. 1, pp. 122 – 125, 2003.

[28] Y. Luo, K. Yakuma, T. Takagi, and S. Maruyama, "Thermal responses of a thermoelectric sma manipulator," *International Journal of Applied Electromagnetics and Mechanics*, vol. 19, no. 1-4, pp. 303 – 307, 2004.

[29] K.-J. Cho and H. H. Asada, "Design of a multi-axis sma actuator arrays using segmented binary control," in *American Society of Mechanical Engineers, Dynamic Systems and Control Division (Publication) DSC*, vol. 73 2 PART B, pp. 1353 – 1358, 2004.

[30] B. Selden, K.-J. Cho, and H. H. Asada, "Segmented binary control of shape memory alloy actuator systems using the peltier effect," in *Proceedings - IEEE International Conference on Robotics and Automation*, no. 5, pp. 4931 – 4936, 2004.

[31] B. Selden, K.-J. Cho, and H. H. Asada, "Multi-segment state coordination for reducing latency time of shape memory alloy actuator systems," in *Proceedings - IEEE International Conference on Robotics and Automation*, vol. 2005, pp. 1350 – 1355, 2005.

[32] B. Selden, K. Cho, and H. H. Asada, "Segmented shape memory alloy actuators using hysteresis loop control," *Smart Materials and Structures*, vol. 15, no. 2, pp. 642 – 652, 2006.

[33] K.-J. Cho, B. Selden, and H. H. Asada, "Segmented binary control of multi-axis sma array actuators," in *Proceedings of SPIE - The International Society for Optical Engineering*, vol. 5757, pp. 314 – 322, 2005.

[34] K.-J. Cho and H. H. Asada, "Architecture design of a multiaxis cellular actuator array using segmented binary control of shape memory alloy," *IEEE Transactions on Robotics*, vol. 22, no. 4, pp. 831 – 843, 2006.

[35] M. Menon and H. H. Asada, "Iterative learning control of shape memory alloy actuators with thermoelectric temperature regulation for a multifunctional car seat," in *Proceedings of the American Control Conference*, vol. 2006, pp. 935 – 939, 2006.

[36] L. Odhner and H. H. Asada, "Shape memory alloy actuator arrays using thermoelectric devices for dual sensing and actuation," in *American Society of Mechanical Engineers, Dynamic Systems and Control Division (Publication) DSC*, vol. 74 DSC 2 PART B, pp. 1683 – 1687, 2005.

[37] B. Sun, J. Zhang, X. Wu, and W. Liao, "Single-joint driving system of bionic finger based on shape memory alloy," in *2012 International Symposium on Micro-NanoMechatronics and Human Science, MHS 2012*, pp. 225 – 228, 2012.

[38] H.-P. Yoong, *Design, Fabrication, Modeling and Control of Artificial Muscle Actuated Wrist Joint System.* PhD thesis, Concordia University, Montreal, Quebec, Canada, November 2018. Ph.D. dissertation, Department of Mechanical, Industrial & Aerospace Engineering.

[39] J. Jeong, K. Hyeon, J. Han, C. H. Park, S.-Y. Ahn, S.-K. Bok, and K.-U. Kyung, "Wrist assisting soft wearable robot with stretchable coolant vessel integrated sma muscle," *IEEE/ASME Transactions on Mechatronics*, vol. 27, no. 2, pp. 1046 – 1058, 2022.

[40] R. Romano and E. A. Tannuri, "Modelling and experimentally validating a shape memory alloy actuator; [modelagem e validação experimental de um atuador baseado em liga de memória de forma]," *Controle y Automacao*, vol. 19, no. 1, pp. 30 – 42, 2008.

[41] R. Romano and E. A. Tannuri, "New development on shape memory alloys actuators," in *BIODEVICES 2008 - Proceedings of the 1st International Conference on Biomedical Electronics and Devices*, vol. 2, pp. 55 – 61, 2008.

[42] R. Romano and E. A. Tannuri, "Modeling, control and experimental validation of a novel actuator based on shape memory alloys," *Mechatronics*, vol. 19, no. 7, pp. 1169 – 1177, 2009.

[43] Y. Wakasa, Y. Watanabe, A. Yoshida, K. Tanaka, and T. Akashi, "Response improvement of shape memory alloy actuators with peltier elements," in *Proceedings of 2008 IEEE International Conference on Mechatronics and Automation, ICMA 2008*, pp. 587 – 592, 2008.

[44] S. Qian, Y. Geng, Y. Wang, J. Ling, Y. Hwang, R. Radermacher, I. Takeuchi, and J. Cui, "A review of elastocaloric cooling: Materials, cycles and system integrations," *International Journal of Refrigeration*, vol. 64, pp. 1 – 19, 2016.

[45] Z. Dong, R. Hou, H. Jiang, W. Wang, F. Zhang, G. Zhao, C. Chen, and P. Ma, "Hybrid thermoelectric-triboelectric smart knitted fabric for real-time monitoring of vascular crisis and post-operative recovery of severed fingers," *Materials and Design*, vol. 251, 2025.

[46] M. Craighero, Q. Li, Z. Zeng, C. Choi, Y. Kim, H. Yoon, T. Liu, P. Sowinski, S. Haraguchi, B. Hwang, B. Mihiretie, S. Fabiano, and C. Müller, "Poly(benzodifurandione) coated silk yarn for thermoelectric textiles," *Advanced Science*, vol. 11, no. 38, 2024.

[47] S. Kim, S. Lim, M. H. Jeong, W. Kim, S. Baik, and J. W. Suk, "Flexible thermocouple using a thermoelectric graphene fiber with a seamless junction," *Journal of Materials Science and Technology*, vol. 172, pp. 15 – 22, 2024.

[48] F. Yin, X. Luo, X. Wang, Y. Liang, T. Wu, Y. Li, and K.-Q. Zhang, "Flexible and air-stable n-type oleylamine/carbon nanotube hybrid yarns for high-performance wearable thermoelectric generators," *Chemical Engineering Journal*, vol. 498, 2024.

[49] H. Hardianto, G. D. Mey, B. Malengier, and L. V. Langenhove, "Textile-based thermoelectric generator fabricated from carbon fibers," *Journal of Industrial Textiles*, vol. 51, no. 5,suppl, pp. 8411–8427, 2022.

[50] X. He, J. Gu, Y. Hao, M. Zheng, L. Wang, J. Yu, and X. Qin, "Continuous manufacture of stretchable and integratable thermoelectric nanofiber yarn for human body energy harvesting and self-powered motion detection," *Chemical Engineering Journal*, vol. 450, 2022.

[51] J. Yang, Y. Pu, H. Yu, D.-d. Ye, X. Liu, and J. H. Xin, "A cross-plane design for wearable thermoelectric generators with high stretchability and output performance," *Small*, vol. 19, no. 45, 2023.

[52] J. Li, B. Xia, X. Xiao, Z. Huang, J. Yin, Y. Jiang, S. Wang, H. Gao, Q. Shi, Y. Xie, and J. Chen, "Stretchable thermoelectric fibers with three-dimensional interconnected porous network for low-grade body heat energy harvesting," *ACS Nano*, vol. 17, no. 19, pp. 19232 – 19241, 2023.

[53] Y.-S. Chen and B.-J. Lwo, "Flexible thermoelectric films by electrospinning," in *2020 15th International Microsystems, Packaging, Assembly and Circuits Technology Conference (IMPACT)*, pp. 219–222, Oct 2020.

[54] G. Karalis, L. Tzounis, K. Tsirka, C. K. Mytafides, M. Liebscher, and A. S. Paipetis, "Carbon fiber/epoxy composite laminates as through-thickness thermoelectric generators," *Composites Science and Technology*, vol. 220, 2022.

[55] A. Panbude, S. Sathiyamoorthy, R. Kumar, H. Shankar, S. Paulraj, V. Kathirvel, A. Adam, E. Ibrahim, K. Jayabal, and P. Veluswamy, "Incorporation of polyaniline on graphene-related materials for wearable thermoelectric applications," *Materials Letters*, vol. 304, 2021.

[56] J. Peng, F. Ge, W. Han, T. Wu, J. Tang, Y. Li, and C. Wang, "Mxene-based thermoelectric fabric integrated with temperature and strain sensing for health monitoring," *Journal of Materials Science and Technology*, vol. 212, pp. 272 – 280, 2025.

[57] J. Dona, S. Harish, K. Hara, and M. Navaneethan, "Metal-assisted growth of mos2 nanosheets on carbon fabric with enhanced electrical conductivity for self-powered wearable thermoelectric application," *Journal of Materials Science: Materials in Electronics*, vol. 34, no. 20, 2023.

[58] U. Farooq, B. Ali, H. C. Bidsorkhi, A. G. D'Aloia, and M. S. Sarto, "Graphene-based flexible thermal sensor and thermopile approach for enhancing thermometry sensitivity in next-generation wearables," *IEEE Sensors Letters*, vol. 8, pp. 1–4, Oct 2024.

[59] I. R. Radulescu, L. Dinca, E. Perdum, C. Stroe, T. Sarbu, and R. M. Aileni, "Thermocouple fabrics for energy harvesting in smart textiles - applications and prototype," in *2023 IEEE 29th International Symposium for Design and Technology in Electronic Packaging (SIITME)*, pp. 223–226, Oct 2023.

[60] A. Golla, G. Schmidl, J. Mersch, A. Gawlik, J. Plentz, L. Hahn, and C. Cherif, "Thermoelectric generator modules based on warp knitted glass fiber-metal hybrid composites," *Materials Research Express*, vol. 11, no. 7, 2024.

[61] S. Newby, W. Mirihanage, and A. Fernando, "Wearable, knitted 3d spacer thermoelectric generator with detachable p-n junctions for body heat energy harvesting," *Sensors*, vol. 24, no. 16, 2024.

[62] Y. Kyosev, "1 - introduction: the main types of braided structure using maypole braiding technology," in *Braiding Technology for Textiles*, Woodhead Publishing Series in Textiles, pp. 1–25, Woodhead Publishing, 2015.

[63] C. Emonts, N. Grigat, F. Merkord, B. Vollbrecht, A. Idrissi, J. Sackmann, and T. Gries, "Innovation in 3d braiding technology and its applications," *Textiles*, vol. 1, no. 2, pp. 185–205, 2021.

[64] C. Zhang, S. Wu, H. Narayana, Y. Ke, H. Shao, E. Zabihi, A. Bahi, N. Chen, P. Servati, J. Jiang, and F. K. Ko, "Programmable 3d bifurcated braided structures for system-adaptable and integrated triboelectric sensing," *Nano Energy*, vol. 118, 2023.

[65] C. Zhang, S. Wu, A. Bahi, H. Narayana, X. Yang, W. Wang, Y. Ke, X. Yin, F. Zabihi, H. Shao, G. Shao, C. Zhou, P. Servati, X. Lu, J. D. Madden, J. Jiang, N. Chen, and F. K. Ko, "Tensile-responsive triboelectric yarn based on janus tubular braided structure for wearable sensing," *Nano Energy*, vol. 131, 2024.

[66] E. Duan, S. A. Jaseem, J. Y. Kim, M. D. Dickey, and M. Bryant, "Strain amplification via helically braided fiber reinforced sleeve for soft material energy harvesting," *Advanced Materials Technologies*, 2025.

[67] Y. Qi, Y. Xue, B. Gu, B. Sun, and W. Zhang, "Dual thermal/electrical-driven compressive recovery behaviors of 3d braided shape memory composite tubes," *Composites Science and Technology*, vol. 233, 2023.

[68] Q. Yang, R. Liu, B. Gu, B. Sun, C. Han, and W. Zhang, "Electrical/thermal triggering on shape memory composite tubes with different braiding angles," *Smart Materials and Structures*, vol. 33, no. 7, 2024.

[69] J. Mersch, C. A. Gómez Cuaran, A. Vasilev, A. Nocke, C. Cherif, and G. Gerlach, "Stretchable and compliant textile strain sensors," *IEEE Sensors Journal*, vol. 21, no. 22, pp. 25632 – 25640, 2021.

[70] Z. Zhang, Y. Jia, J. Che, P. Liu, and Y. Gong, "The effects of manufacturing parameters on static characteristics of water hydraulic artificial muscles," *IEEE Access*, vol. 8, pp. 200669–200679, 2020.

[71] S. Lee and J. Lee, "Braided fabrication of a fiber bragg grating sensor," *Sensors (Switzerland)*, vol. 20, no. 18, pp. 1 – 17, 2020.

[72] W. Tian, S. Wakimoto, D. Yamaguchi, and T. Kanda, "Fabrication process for twisting artificial muscles by utilizing braiding technology and water-soluble fibers," *IEEE Robotics and Automation Letters*, vol. 9, no. 4, pp. 3147 – 3154, 2024.

[73] T. Masselter, O. Speck, and T. Speck, "3d reticulated actuator inspired by plant up-righting movement through a cortical fiber network," *Biomimetics*, vol. 6, no. 2, 2021.

[74] J. McAfee and N. Faisal, "Parametric sensitivity analysis to maximise auxetic effect of polymeric fibre based helical yarn," *Composite Structures*, vol. 162, Nov 2016.

[75] M. A. Hoque, E. Petersen, and X. Fang, "Effect of material properties on fiber-shaped pneumatic actuators performance," *Actuators*, vol. 12, no. 3, 2023.

[76] S. Kandasamy, M. Teo, N. Ravichandran, A. McDaid, K. Jayaraman, and K. Aw, "Body-powered and portable soft hydraulic actuators as prosthetic hands," *Robotics*, vol. 11, no. 4, 2022.

[77] R. Wu, S. Liu, Z. Lin, S. Zhu, L. Ma, and Z. L. Wang, "Industrial fabrication of 3d braided stretchable hierarchical interlocked fancy-yarn triboelectric nanogenerator for self-powered smart fitness system," *Advanced Energy Materials*, vol. 12, no. 31, 2022.

[78] H. Dong, C. Zhi, C. Wang, R. Sun, Z. Dong, Y. Zhang, C. Xu, H. Guo, M. Ren, Y. Xu, M. Zhang, and L. Yu, "Artificial vascular stent-inspired bending sensors embedded in a data glove for hand gesture recognition," *IEEE Sensors Journal*, vol. 23, pp. 23388–23398, Oct 2023.

[79] O. Rufai, M. Gautam, P. Potluri, and M. Gresil, "Optimisation of optical fibre using micro-braiding for structural health monitoring," *Journal of Intelligent Material Systems and Structures*, vol. 30, no. 2, pp. 171–185, 2019.

[80] P. Lugoda, J. C. Costa, C. Oliveira, L. A. Garcia-Garcia, S. D. Wickramasinghe, A. Pouryazdan, D. Roggen, T. Dias, and N. Münzenrieder, "Flexible temperature sensor integration into e-textiles using different industrial yarn fabrication processes," *Sensors (Switzerland)*, vol. 20, no. 1, 2020.

[81] X. Wang, H. Shao, J. Tang, J. Chen, Y. Huang, J. Pan, Y. Zhang, W. Wang, J. Jiang, and N. Chen, "Braided liquid crystal elastomer fiber actuator with programmable deformation for artificial muscles," *Advanced Materials Technologies*, vol. 8, no. 19, 2023.

[82] D. Madheswaran, M. Sivan, S. Hauzerova, E. K. Kostakova, V. Jencova, J. Valtera, L. Behalek, J. Mullerova, N. H. Nguyen, L. Capek, and D. Lukas, "Continuous fabrication of braided composite nanofibrous surgical yarns using advanced ac electrospinning and braiding technology," *Composites Communications*, vol. 48, 2024.

[83] R. K. Seidu and S. Jiang, "Performance quality of braided e-yarns for pedestrian interactive textiles," *Engineering Proceedings*, vol. 52, no. 1, 2023.

[84] H. J. Yang, J. Y. Lee, and W.-R. Yu, "Carbon nanotube fiber assemblies with braided insulation layers for washable capacitive textile touch sensors," *Functional Composites and Structures*, vol. 2, no. 1, 2020.

[85] Y. Yoshimoto, S. Wakimoto, W. Tian, K. Inoue, D. Yamaguchi, and T. Kanda, "Combination process of a pneumatic artificial muscle and a fiber optical sensor system †," *Engineering Proceedings*, vol. 27, no. 1, 2022.

[86] B. Napier, G. Matzeu, and F. G. Omenetto, "Multi-sensing yarns for continuous wireless sweat lactate monitoring," *Communications Materials*, vol. 5, no. 1, 2024.

[87] H. Gong, Z. Peng, Y. Liu, Z. Chen, S. Fei, R. Xu, K. Liu, D. Xu, and Y. Guo, "Fire-retardant braided electronic rope with a hierarchical core-shell structure for fire rescue operations," *Composites Part B: Engineering*, vol. 271, 2024.

[88] H. Le Xuan, E. Haentzsche, A. Nocke, N. H. A. Tran, I. Kruppke, and C. Cherif, "Development of fiber-based piezoelectric sensors for the load monitoring of dynamically stressed fiber-reinforced composites," *Smart Materials and Structures*, vol. 32, no. 4, 2023.

[89] Y. Tajitsu, J. Takarada, T. Hikichi, R. Sugii, K. Takatani, H. Yanagimoto, R. Nakanishi, S. Shiomi, D. Kitamoto, T. Nakiri, O. Takeuchi, M. Deguchi, T. Muto, K. Kuroki, W. Amano, A. Misumi, M. Takahashi, K. Sugiyama, A. Tanabe, S. Kamohara, R. Nisho, and K. Takeshita, "Application of piezoelectric plla braided cord as wearable sensor to realize monitoring system for indoor dogs with less physical or mental stress," *Micromachines*, vol. 14, no. 1, 2023.

[90] Y. Liu, L. Li, F. Xiao, R. Hou, Z. Lin, X. Cai, S. Zuo, Y. Zhou, S. Hua, Y. Chen, and X. Jin, "Braided niti alloys microfilaments with near-linear responses: Toward flexible high-pressure sensors," *Journal of Materials Science and Technology*, vol. 229, pp. 269 – 278, 2025.

[91] Y. Tajitsu, S. Shimda, T. Nonomura, H. Yanagimoto, S. Nakamura, R. Ueshima, M. Kawanobe, T. Nakiri, J. Takarada, O. Takeuchi, R. Nisho, K. Takeshita, M. Takahashi, and K. Sugiyama, "Application of braided piezoelectric poly-l-lactic acid cord sensor to sleep bruxism detection system with less physical or mental stress," *Micromachines*, vol. 15, no. 1, 2024.

[92] A. Pragya, H. Singh, B. Kumar, H. Gupta, and P. Shankar, "Designing and investigation of braided-cum-woven structure for wearable heating textile," *Engineering Research Express*, vol. 2, no. 1, 2020.

[93] B. Chaudhary, H. Matos, S. Das, and J. Owens, "Multifunctional composite structures with embedded conductive yarns for shock load monitoring and failure detection," *Smart Materials and Structures*, vol. 33, no. 3, 2024.

[94] A. Hardianto, B. Malengier, G. Mey, L. Van Langenhove, and C. Hertleer, "Textile yarn thermocouples for use in fabrics," *Journal of engineered fibers and fabrics*, vol. 14, March 2019.

[95] Fraens, "3d printed braiding machine / how it works, construction, technical details," January 2021. Accessed: 2025-06-06.

[96] Jack, "Braiding machine." `https://www.printables.com/model/385305-braiding-machine`, January 2024. Accessed: 2025-06-06.

[97] C. B. Churchill and J. A. Shaw, "Shakedown response of conditioned shape memory alloy wire," in *Proceedings of SPIE - The International Society for Optical Engineering*, vol. 6929, 2008.

[98] P. Fieguth, *An Introduction to Complex Systems: Society, Ecology, and Nonlinear Dynamics.* Springer International Publishing, 2016.

[99] B. Hanington and B. Martin, *Universal Methods of Design: 100 Ways to Research Complex Problems, Develop Innovative Ideas, and Design Effective Solutions.* Rockport Publishers, 2012.

A

Literature search and filtering strategy

Three topics were explored in the literature review and state-of-the-art found in Section 1.2, and the specific strategy and research process for each topic is explained in this appendix. OpenAI's ChatGPT (May 2024 version) is a large language model that assisted in synthesizing literature review abstracts and processing relevance-based exclusion filters. The model was fed a list of papers and their abstracts in the form of a plain text bibtex bibliography entry with abstracts, and the model generated two spreadsheets (one for rejected papers and one for included papers) with a brief justification by the model for their inclusion in either spreadsheet. Manual filtering took place from there, where the justification was considered and a final decision regarding inclusion or exclusion was made.

Thermoelectric cooling methods for SMAs

This report uses the following search query to review the intersection of thermoelectric cooling and shape memory alloys: ((”shape memory alloy” OR sma OR nitinol) AND (thermoelectric OR peltier) AND (cooling OR (thermal AND control))). Literature selection focused on studies where active thermal management — specifically Peltier-based thermoelectric cooling — was applied to enhance SMA actuator performance. Priority was given to research demonstrating how active cooling influenced key performance metrics such as actuation bandwidth, response time, cycle frequency, force output, or fatigue life. Studies limited to passive cooling methods (ambient airflow, conduction to heat sinks) were excluded, as were papers focused solely on SMA alloy development or phase transformation modeling without any active thermal control component. In addition, it was noted during the review that elastocaloric cooling has emerged as a strong competing strategy to thermoelectric cooling, and one review article on ths subject was selected for inclusion. The resulting literature review provides a targeted overview of Peltier-cooled SMA systems and their limitations, directly informing this thesis's exploration of textile-integrated thermoelectric cooling for wearable SMA actuators.

Textile integration of thermoelectric devices

Papers with this topic were found using the following search query: ((”thermoelectric” OR ”Peltier”) AND (textile OR fabric OR yarn OR knit) AND (integration OR wearable OR embedded)) On Scopus, this query returned 118 English-language articles published within the past five years in the field of Engineering. The same query on IEEE Xplore identified an additional 24 unique articles. After removing duplicates, 142 articles were screened for relevance. The filtering criteria prioritized studies involving flexible, yarn- or fiber-based TE materials that were structurally integrated into textile architectures — particularly woven, knitted, or braided forms. Special emphasis was placed on work demonstrating active cooling applications (Peltier effect), though Seebeck-based power generation papers were included when they presented insights into textile-compatible TE integration methods. Papers were excluded if the TE device remained a rigid module simply affixed to the textile surface, or if the textile served only as a passive carrier with no mechanical or functional integration. Studies focused solely on nanomaterial synthesis or thermoelectric ink printing were retained only when clear strategies for textile implementation were demonstrated. After filtering, 22 papers were retained and further examined in the literature review to inform the development of braided, textile-integrated TE cooling architectures.

Braided smart textiles

The following search query: (braid* AND (textile OR yarn OR fiber)) AND ("smart textile" OR e-textile OR "intelligent textile" OR sensor OR actuator OR "wearable device") On Scopus, this query returned 72 English-language articles published within the past five years in the field of Engineering. The same query on IEEE Xplore produced an additional 14 unique articles. After deduplication, 86 articles were screened for relevance. The filtering process prioritized papers that explored functional uses of braided structures in wearable, responsive, or sensor-enabled systems — especially those leveraging braiding to influence mechanical behavior (strain distribution, stiffness), fiber alignment, electrical integration, or actuation performance. Articles focused solely on non-functional industrial applications (e.g., cable sheathing, protective sleeves, braid inspection) were excluded. Borderline papers were retained if they demonstrated novel uses of braiding in sensing, actuation, or smart material integration with potential applicability to wearable devices. The final selection reflects a focused survey of braided textile structures relevant to the goal of developing a braided architecture capable of integrating both thermoelectric and shape-memory alloy elements, as pursued in this thesis.

B

Detailed results and data

(a) Control

(b) Passive Peltier sheath

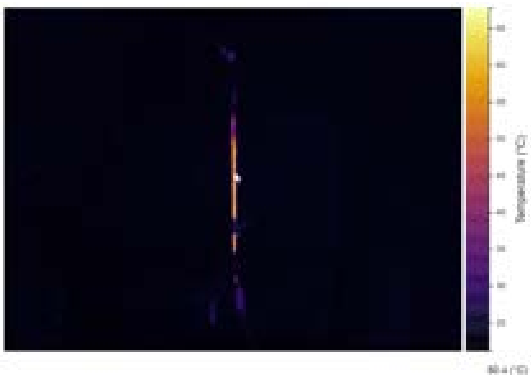

(c) Peltier-only cycling

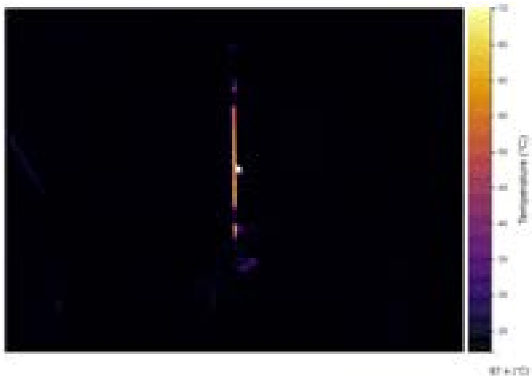

(d) Resistive heating with Peltier cooling

Figure B.1: Thermal photos of peak temperature for configurations with resistive heating

Figure B.1 represents the thermal imaging results of different test configurations, illustrating the temperature distribution across control and Peltier-integrated setups during resistive heating cycles at their respective peak temperatures. Figure B.2 presents the recorded voltage and force signals across the four primary test configurations. Each subplot shows the SMA activation voltage, the voltage across the conductive sheath, and the measured force as a function of time. These plots provide a comparative view of the system behavior under different combinations of heating and cooling inputs.

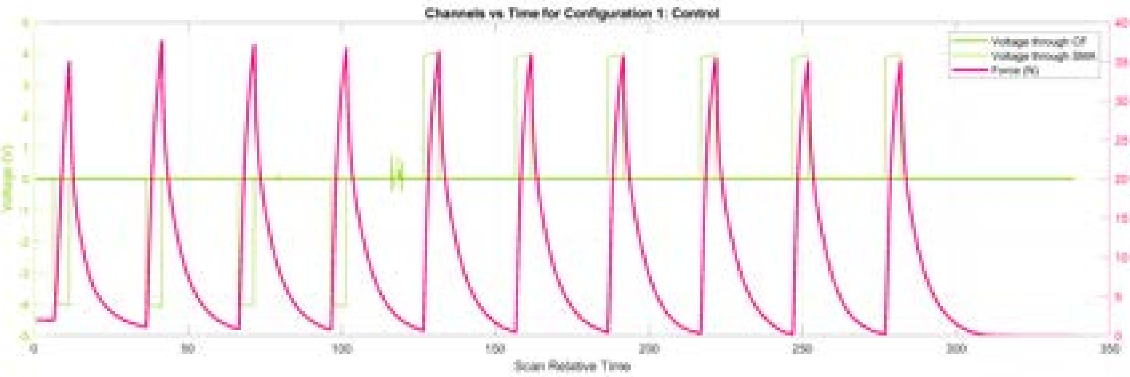

(a) Control

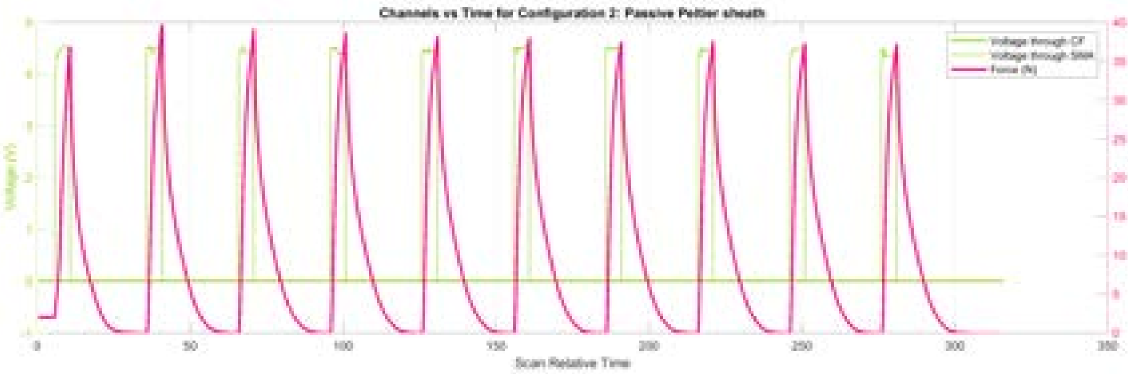

(b) Passive Peltier sheath

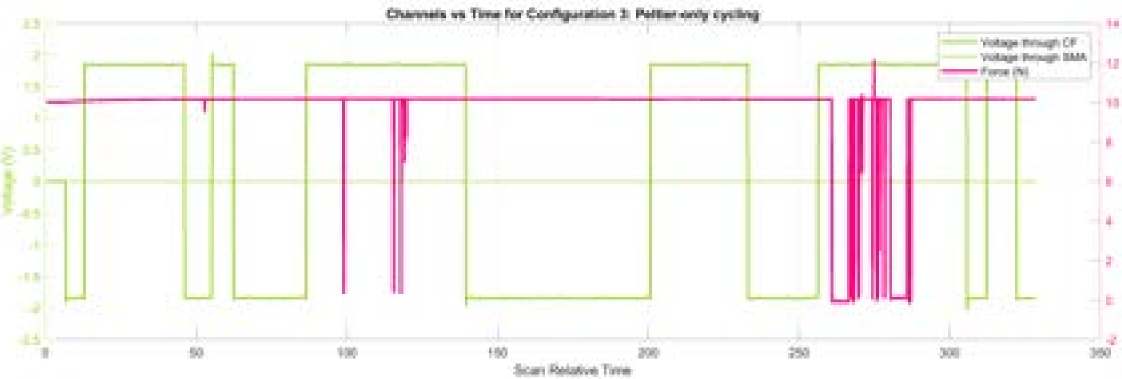

(c) Peltier-only cycling

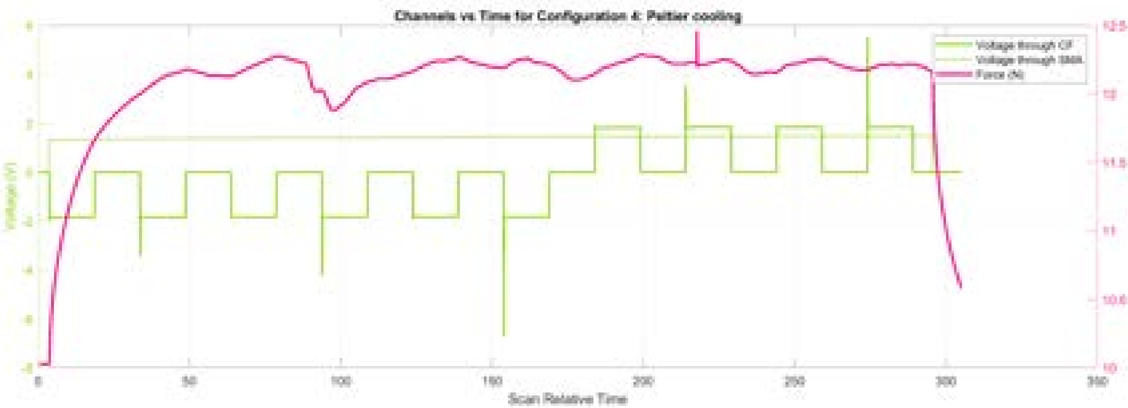

(d) Resistive heating with Peltier cooling

Figure B.2: Voltage and force measurements over time for each test configuration

Configuration 1 and 2 – T-test results for area under the curve between control and Peltier sheath response

```
Mean AUC - Control: 96.4864 ± 1.4657
Mean AUC - Peltier: 95.6709 ± 13.3137
Two-sample t-test p = 0.8849
→ No significant difference in AUC between Peltier and Control.
```

Configuration 4 – T-test results for area under the curve between Peltier cooling and Peltier heating

```
Mean AUC - Cooling: 0.3289 ± 0.1193
Mean AUC - Heating: 0.3968 ± 0.1428
Two-sample t-test p = 0.5364
→ No significant difference in AUC between heating and cooling.
```

This page is intentionally left blank.

This page is intentionally left blank.

This page is intentionally left blank.